Photocatalytic Properties of SiO_2 coated Degussa P25 TiO_2 Powder by Scalable Atomic Layer Deposition

Yanchen Song - 4460871

Delft University of Technology

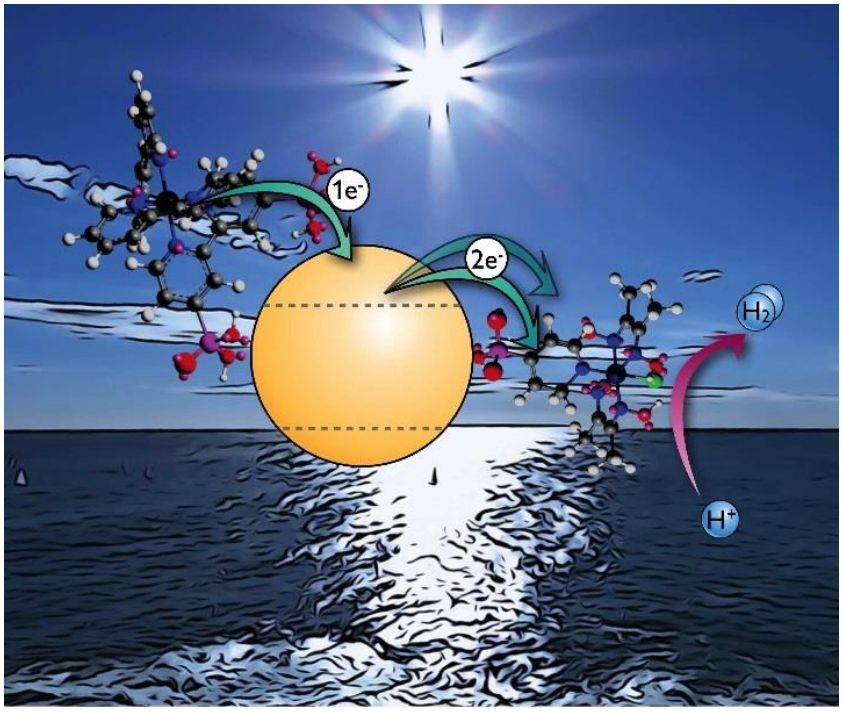

Master Thesis

Photocatalytic Properties of SiO_2 coated Degussa P25 TiO_2 Nanoparticles by Scalable Atmospheric Pressure Atomic Layer Deposition

By

Yanchen Song
4460871

in partial fulfillment of the requirements for the degree of

Master of Science

in Materials Science and Engineering

at the Delft University of Technology,

to be defended on Tuesday April 23rd, 2017 at 13:00.

Supervisor:	Prof. dr. ir. J. R. van Ommen,	TU Delft
	Dr. Hao Van Bui	TU Delft
Thesis committee:	Prof. dr. ir. A. J. Böttger	TU Delft

Abstract

A precise control for the growth of thin film powered by atmospheric pressure atomic layer deposition (ALD) carried out in fluidized bed reactor makes the ultrathin conformal coating of SiO_2 on Degussa P25 TiO_2 nanoparticles possible. At an operating temperature which can be lowered to room temperature (~27°C), the growth per cycle (GPC) smaller than 1 angstrom (~0.8 Å) allowed us to study on the relationship between the thickness of SiO_2 thin film and photocatalytic activities of SiO_2 coated TiO_2 nanoparticles. Importantly, a considerable enhancement of photocatalytic activity was found which resulted from the formation of crosslinking of Si-O-Ti bonds in the interface between SiO_2 and P25 TiO_2 nanoparticles as indicated by XPS and FT-IR. The band gap of this interfacial layer can be tuned from 3.10 to 3.23 eV slightly narrower than P25 TiO_2's by varying the number of ALD cycles and the ALD processes at different temperature corresponding to the thickness of SiO_2 thin film. Such band gap led to a red-shift of the absorption spectra which means the better absorption of visible light and enhanced the charge transfer from TiO_2 to the interface, thereby prevented the rapid recombination of generated carriers. As for the precursors $SiCl_4$ and deionized water vapor, the saturating state of dosing at the first stage of ALD process related to self-limiting reaction can be got after 5 seconds. In addition, annealing could also enable the enhancement of photocatalytic activity via modifying the morphology of interface. Practically speaking, our approach provided a scalable, energy effective and precise method to tune the photocatalytic properties of SiO_2 coated Degussa P25 TiO_2 nanoparticles which can be both used for photocatalyst about enhancement and pigment about suppression.

Keywords: Atomic Layer Deposition, Si-O-Ti interface, self-limiting reaction, photocatalysis, ultrathin conformal SiO_2 film.

Table of Contents

List of Figures

List of Tables

Acknowledgements

During the happy time doing my master project, I learned a lot from this project as well as the people who gave me lots of help and advices in PPE group. The experimental operation, scientific way of thinking and academic analysis make me feel full of energy to study and interested.

Foremost, I would like to express my sincere gratitude to my supervisors Prof. J. Ruud van Ommen and Dr. Amarante Bottger who gave me this unique opportunity to studied on such an interesting topic about photocatalyst. I would like to thank Dr. Hao Van Bui for his continuous support, for his patience, motivation, enthusiasm, and immense knowledge. I would also like to express my thanks to the people of the groups I had the pleasure to work in, namely Product and Process Engineering group of Chemical Engineering and worked happily with Mojgan Talebi, Jing Guo, Fabio Grillo and Damiano la Zara. Thank Mojgan for the patient help about ALD set-up, Jing for the instructions and useful experience, Fabio for the construction of theories and Damiano for the help of undertaking the XPS and INAA tests. It my honor to work with you all!

Finally, I would like to thank my parents and sister for the solid spiritual support across my whole life.

Chapter I

1. Introduction

As an excellent photocatalyst, the catalytic activity of TiO_2 was discovered by Fujishima et al. in 1972. [37] Since then, this kind of materials are used in many industrial fields such a purification of water and air pollution, hydrogen evolution and photoelectrochemical conversion due to its nontoxicity, excellent structural and chemical stability and abundant supply. [38] However because of the relatively wide band gap (~3.2eV), TiO_2 is not capable for harvesting efficiently sunlight in the visible and infrared range to generate sufficient photon flux. [39] In the field of photocatalyst, doping and surface modification are addressed to enhance harvesting efficiency and prevent rapid recombination of charge carriers (e.g., holes and electrons). Doping in some cases can tune the electronic properties as create mid-band gap which is easier to excite electrons or holes due to the lower demand of energy resulting in a red-shift of optical absorption. [40] Additionally, doping accompanying with defects can trap the excited carriers to prevent rapid recombination. [41] Surface modification such as ultrathin films and nanoclusters made by metals or metal oxides serves as another approach to enhance the photocatalytic activities by reducing the charge combination. [41] Growth of Pt islands on the surface of TiO_2 is a good example to achieve enhancement and it's explained that Pt NPs act as the conduction band electron sink due to its lower Fermi level. [42]

Previously, silicon dioxide (SiO_2) was used for supressing the photocatalytic activities of TiO_2 due to its large band gap (~ 9eV) which will block the charge transfer from TiO_2 to surface. Nevertheless, it is reported that the TiO_2-SiO_2 binary system could enhance the photocatalytic activity which is attributed to the presence of silica promote the absorption of dye materials and the active oxygen species could react near the interface between two different materials. Moreover, the presence of Si-O-Ti interfacial layer gives a narrower band gap which could alter the absorption of lights and charge recombination. [31, 32] However, it is quite hard to coat an ultrathin SiO_2 film on nanoparticles which will enable the crosslinking of Si-O-Ti bonds in the interfacial layer to compensate suppression by blocking active sites and reducing of charge transfer and enhance the photocatalytic activity further via wet-chemical methods or general CVD.

1.1 Atomic Layer Deposition

1.1.1 General ALD

In the past decades, liquid-phase epitaxy plays an important role of synthesis in the field of Nano-materials owing to the simplicity. However, the restrictions of this method like limited morphology (crystal orientation) control, rough surface and poor dimensional control make gas-phase more attractive. Atomic layer deposition (ALD) is a gas-phase based technique to meet the requirement of atomic control and conformal deposition which could fabricate inorganic ultrathin layers and chemisorption between monolayers enables much better adhesion than chemical vapor deposition (CVD) which could avoid exfoliation of layers. Based on the sequential self-limiting reactions, one characteristic ALD cycle consists of the following steps which are shown as Figure 1.1.

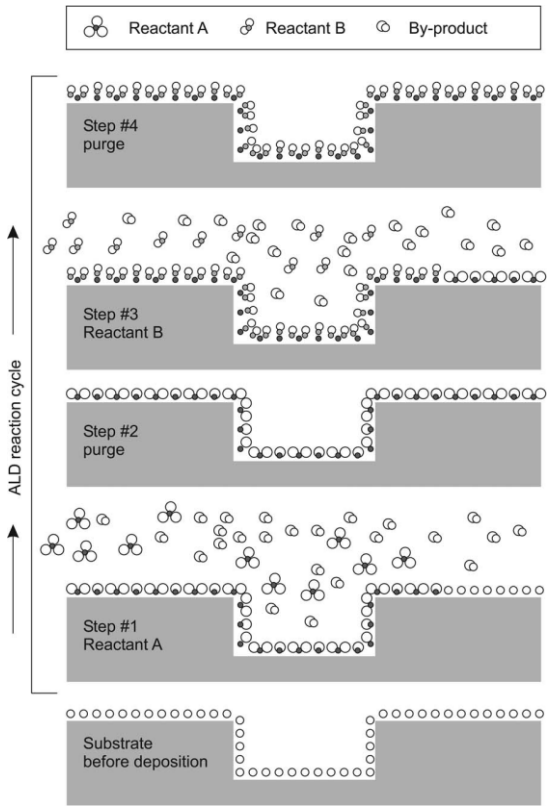

Figure 1. Schematic illustration of one ALD reaction cycle. [1]

Self-limiting reaction occurs in step 1 that the reactant A contact the surface of substrate in finite sites for a short time. In order to remove the by-products and non-reacted reactants, the first purge is applied followed by the second self-limiting reaction of the second reactants or surface treatment to activate the surface sites again like oxidization. After a relatively long purge with the same function of the first purge, one ALD cycle is finished. In addition, for some

inert substrate materials, surface treatments or heat treatments are required before the beginning of the ALD process. The growth of the thin film by means of ALD is identified as growth per cycle (GPC).

The surface chemistry of ALD is mainly about the self-limiting reaction where the adsorption counts. If the surface area adsorbs enough reactant to react and cover the whole surface, the reaction will not proceed anymore. Adsorption could be divided into two interactions phsisorption and chemisorption. The former one is caused by landing of molecules or atoms on the substrate which is weak interaction in this case and it is always reversible. The latter one is dominant which is determined by three main classes: ligand exchange, dissociation and association. As is shown in Figure 1.2, 1) Ligand exchange: The reactant molecules are split which the combination of ligand and surface group forms a new compound and release the by-product in the meantime. 2) Dissociation: the split molecule forms new ligands with the active sites on the surface without releasing gaseous by-products. 3) Association: the molecule forms a coordinative bond with one active site and does not dissociate the ligand. [1]

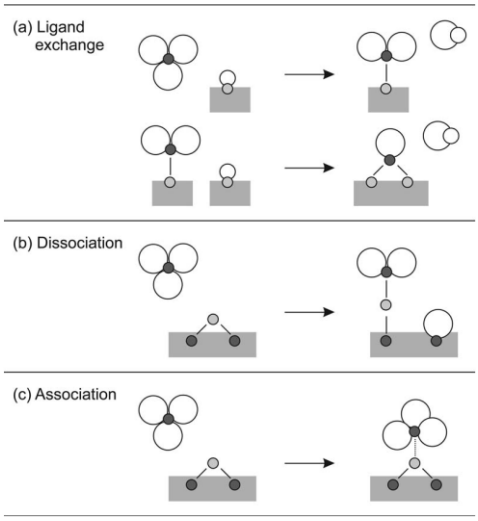

Figure 1-1 Chemisorption mechanisms identified for ALD: a) ligand exchange, b) dissociation, and c) association.

One advantage of ALD is the precise thickness control at monoatomic scale due to the self-limiting reaction to grow one monolayer per cycle. Moreover, the ultrathin film fabricated by ALD is very smooth and conformal to the substrate since there are no active site on the surface left after the reaction reached completion. The extremely homogenous and continuous film without pinhole is vital for dielectric applications. Last but not least, the growth of thin film is independent of substrate's geometry because gaseous precursor will fill the whole space in the chamber or column which means the thin film will form all around the surface of the substrate with the same thickness.

1.1.2 ALD in Fluidized Bed Reactor

For ALD of coating on nanoparticles, usually we use fluidized bed reactor due to the good solid mixing, good heat transfer and ease of process control. Moreover, absence of solvent reduces the waste generated in ALD process. There are three following representative processes of atomic layer deposition in fluidized bed reactor.

1.1.2.1 Deposit Al_2O_3 on TiO_2 nanoparticles

As one of the most representative processes of ALD, deposition of Al_2O_3 on substrates has lot of outstanding characteristics. TMA/Water process is the most frequently used method to fabricate Al_2O_3 in which TMA is really reactive for self-limiting reaction and other gaseous products are rather inert. David et al. has studied the growth mechanism of depositing Al_2O_3 on nanoparticles (TiO_2) at room temperature and atmospheric pressure as well. They found the dosing time, in other words, the dosage of the first precursor (TMA) play a vital role of growth control which the GPC increased not linearly with dosing time as shown in Fig. 1.4 and the GPC is roughly 0.14-0.15nm while it's 0.16nm at 170 °C. If excess precursor is applied, it will make the whole process more like chemical vapor deposition owing to the phsisorption of molecules on the nanoparticles especially at room temperature. In addition, high working temperature induces different surface adhesion of molecules which means most of the phsisorption could be avoided. In Fig.1.3, the films they obtained are quite uniform and the thicknesses also match the data of GPC they got as mentioned above. For applications, these oxide layer could be used as passive barrier or in the field of catalyst, sensor and energy conversion/storage.

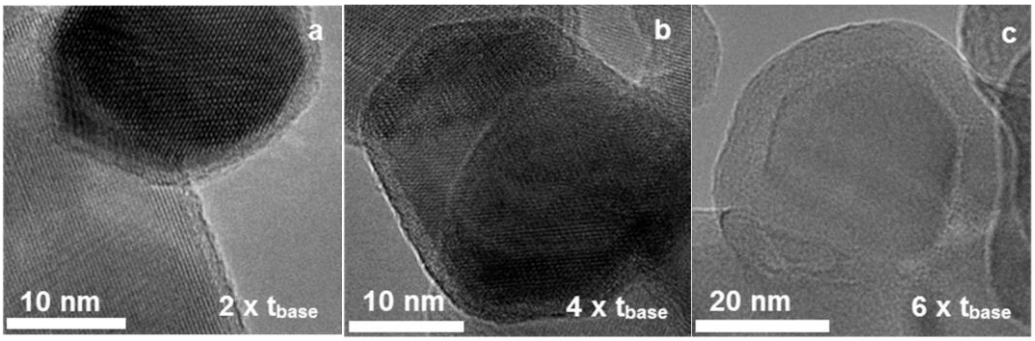

Figure 1-2 TEM images of the alumina film on TiO_2 nanoparticles after 7 cycles when the dosing time of TMA per cycle are (a) 7 min; (b) 14 min; and (c) 21 min. [9]

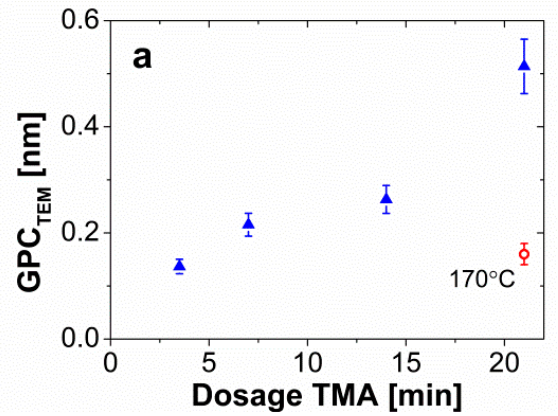

Figure 1-3 GPC of the alumina film on TiO_2 nanoparticles after 7 cycles when the dosing time is different (3.5, 7, 14 and 21 min). Red cycle represents experimental GPC with a dosing time 21min at 170^{o}C

If the density of thin film is relatively low, it might indicate the presence of interior unreacted precursors or porosity. After thermogravimetric analysis (TGA) of the samples, it is obvious that when the reaction temperature is high, accumulation water inside the thin film is low and vice versa. Meanwhile, both of the water's mass losses at high (<0.5%) and low (<0.1%) temperature and that of methyl groups are much lower than uncoated TiO_2. In a nutshell, the low density they found doesn't result from porosity or unreacted precursors.

1.1.2.2 Deposit Pt on TiO_2 nanoparticles

Deposition of platinum clusters on TiO_2 nanoparticles is another interesting point of view. Using $MeCpPtMe_3$ and ozone as reactants, this process is under a relatively low temperature, 250 °C and atmospheric pressure. Aristeidis et al. found Pt islands formed at the substrate while dispersed uniformly in fluidized bed reactor. But at such a low pressure, mixing is much worse especially in a large-scale system reported previously which does bad to several properties. In Aris's research, ozone worked as the oxidizers that could solve this problem mostly at atmospheric pressure. Varying dosing time and number of cycles time allowed the precise control to get homogenously distributed and highly dispersed Pt nanoclusters with small size of particles. In this case, the synthesis of catalyst with excellent performance is achieved.

1.2 SiO_2 thin film deposition

For silica thin film deposition, there are three representatives which are widely used such as wet chemical method (e.g. sol-gel), chemical vapor deposition(CVD) and atomic layer deposition(ALD). It is vital to weigh the pros and cons among different methods in order to meet the requirements for the applications especially for photocatalysis.

1.2.1 Wet-chemical deposition of SiO_2

Sol-gel is the most widely used method for deposition of thin film due to the simple route and low cost. Marage et al. reported commonly used method of depositing silica thin film which were fabricated by the sol-gel technique using tetraethylorthosilicate (TEOS) as a precursor. The introduction of glacial acetic acid at the molar ratio TEOS: acetic acid 1:15 causes acetate modification, resulting in an exothermic reaction and the solution is modified by a small amount of water later on. Acetylacetone acts as a stabilizer, hence it is added in the molar ratio TEOS: acetylacetone 1:1. Different molar content of TEOS enables the deposition of SiO_2 layers with different thickness. [12] Such wet chemical deposition has the following pros: 1. Cost effective; 2. No need of vacuum equipment; 3. Roughly control of coverage and thickness.

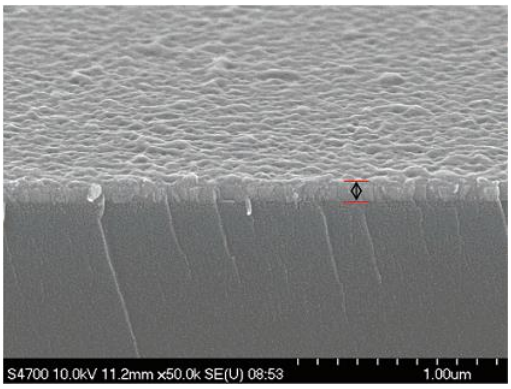

Figure 1-4 SEM of SiO_2 film [13]

Generally, the thickness of silica thin film fabricated by sol-gel is about 100nm which could be seen in Fig. 1.5. However, the quality of silica film is quite poor owing to the porosity which will result in the poor electronic properties and stability. As for the morphology, it is characterized by AFM according to the variation of the volume ratio of EtOH:TEOS as shown in Fig. 1.6.

In order to avoid porosity, another similar method is going to be used as sol electrophoretic deposition (EPD) which requires a reactor to allow the colloidal particles suspended in a liquid medium migrate under the influence of an electric field which the process is so called electrophoresis and are deposited onto an electrode while the rest is almost the same as sol-gel method. But the surface of substrate must be electrically conductive. The precise control of growth compared with normal sol-gel make low reacting temperature and ultra-thin film(~5nm) [15] possible to get better dielectric properties. From the figure above, on the one hand, it is obvious that the pores will become larger and smaller if the volume ratio of EtOH and TEOS is decreased and the pores almost disappear when the ratio decreased to 2:1. On the other hand, after heat treatment, the film surface gets much flatter and smoother as well as EPD.

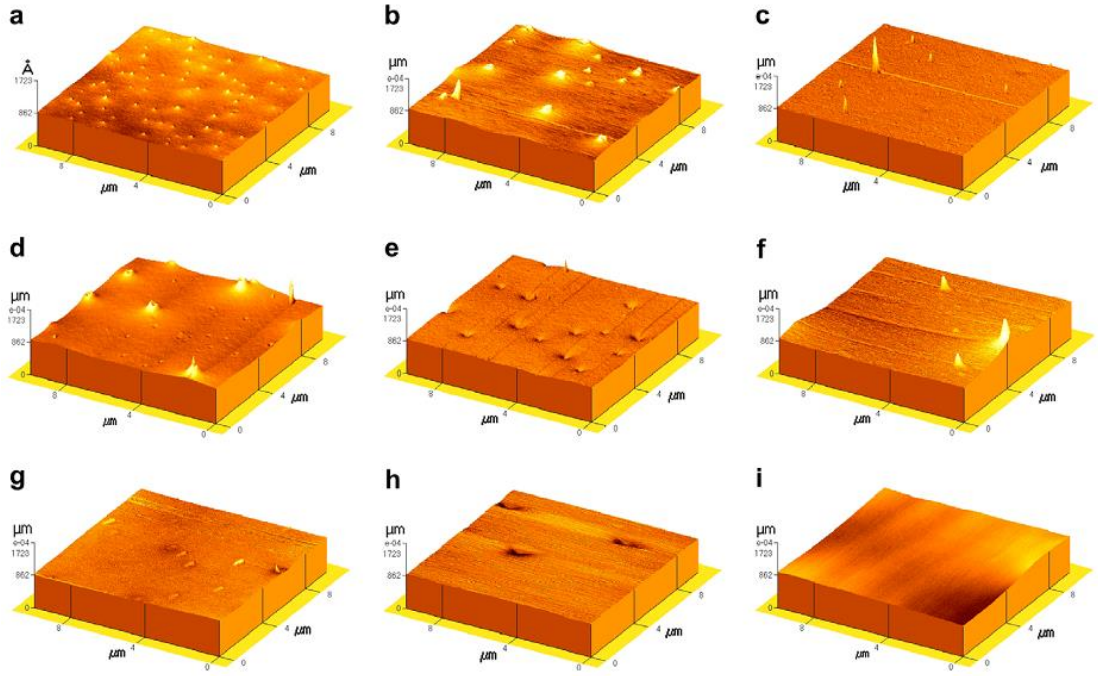

Figure 1-5 The surface morphology of the sol–gel and the EPD SiO_2 films. The films were processed using the following conditions, EtOH:TEOS volume ratio: (a) 10:1, without annealing, (b) 10:1, annealing for 1 h at 100°C, (c) 10:1, EPD for 72 h with annealing for 1 h at 100°C, (d) 5:1, without annealing, (e) 5:1, with annealing for 1 h at 100°C, (f) 5:1, EPD for 72 h with annealing for 1 h at 100°C, (g) 2:1, without annealing, (h) 2:1, with annealing for 1 h at 100°C and (i) 2:1, EPD for 72 h with annealing for 1 h at 100°C. [14]

1.2.2 CVD of SiO_2

Chemical vapor deposition(CVD) which is used to fabricate various insulator films is paramount in semiconductor industries. In general, chemical vapor deposition of some insulator thin film is proceeded under very high temperature(700-1200 °C) and relatively high pressure. The film is more uniform than the one made by so-gel method while for the film coated on high radius of curvature substrate like nanoparticle, the thin film quality is not that good as flat substrate as shown in Fig. 1.7 and the thickness is about from 10nm-60nm normally.

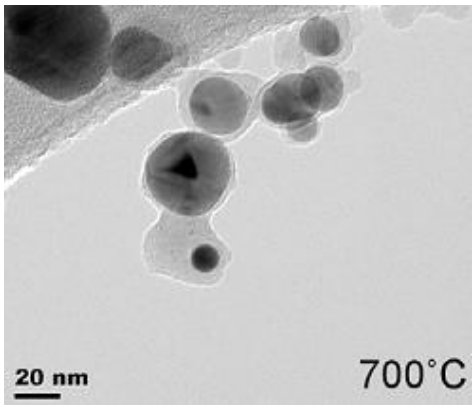

Figure 1-6 TEM of SiO_2 coated Silver nanoparticle [17]

Recently, K. Maeda et al. proposed mixing precursor TEOS(tetraethylorthosilicate) with ozone in the presence of relatively high temperatures under atmospheric pressure. In this case, the growth of uniform silica film at 400 °C with growth rates of 0.1 μm/min or more could be achieved. The process could be described as the reaction below. [16]

$$Si(OC_2H_5)_4 + 4O_3 \rightarrow SiO_2 + 10H_2O + 8CO_2 + by - producct\ \ mixtures \quad (1.1)$$

Water as an undesirable residue is quite hard to be removed unless heated to 500 °C while the moisture consisting of oxides which are reflowed or densified at relatively high temperature could be eliminated. The advantage of CVD provided by this process are the excellent step coverage and in-situ flow owing to the surface mobility prior to formation of silica. In addition, the film thickness uniformity could also be enhanced by precise control of reactant injector temperature and by-product exhaust systems.

1.2.3 ALD of SiO_2

As a precise controlling deposition technique, ALD exhibits saturation growth behavior and the thickness of SiO_2 thin film could be lowered to several angstroms based on self-limiting and sequential surface reactions while the GPC is about 1 Å. Previously, volatile silanes with halogen, alkyl and alkoxy ligands are used as the silicon sources. [23,24]

Table 1-1 Parameters of commonly used combination of precursors for ALD-SiO_2

1st Precursor	Oxidizer	Temperature	Pressure	Ref.
Tetramethyl orthosilicate [$Si(OCH_3)_4$]	Water vapor	150°C	10-20mTorr	18
Tetrakis(ethylamino)silane [$Si(NHC_2H_5)_4$]	Ozone	325-514°C	2-9.5Torr	19
Tris-dimethylaminosilane [$SiH(N(CH_3)_2)_3$]	H_2O_2	100-250°C	2.25-3Torr	20
Silicon tetrachloride [$SiCl_4$]	Water vapor	320-420°C	1-1.3Torr	21
$H_2Si[N(C_2H_5)_2]_2$	O_2 plasma	50-400°C	150mTorr	22

Nowadays, due to the wide range of structural variations, better safety protection and higher chemical reactivity, new combination of precursors are used. Some commonly used experimental conditions and chemicals are shown in the following table 1.1.

It is easy to find that some of the precursors need vacuum conditions such as tetramethyl orthosilicate and others need high pressures saying tetrakis(ethylamino)silane and tris-dimethylaminosilane. For the pair of silicon tetrachloride and water vapor, it is both under low temperature and low pressure (atmospheric pressure) and the ultrathin layer can be varied from 0.7nm as shown in Fig. 1.8 to several nanometers. Morphology of SiO_2 ultrathin film fabricated by ALD can be quite uniform. A low deposition temperature below a certain level may limit the growth due to the energy for chemisorption which means it requires longer deposition time. If the deposition temperature increases to a certain level, such sufficient thermal energy will result in a situation that more absorbed precursor covered on the surface increases the Si-O bond while most of the hydroxyl bonded water is lost and hydroxyl condensation will occur. From the previous work, high density and low surface roughness of SiO_2 film via ALD can be observed at high temperature and vice versa. In the same manner, selection of specific precursor is very important for the synthesis process because evaporation temperature and pressure effects the coverage and quality of thin films. In ALD process, operating pressure and partial pressure of precursors influences the reaction path and partial pressures of carrier gas and by-production are very sensitive to the growth of thin films. Technically high pressure can stabilize adsorbates thermodynamically or it will desorb at low pressure. Based on the information given above, silicon tetrachloride and water vapor can achieve good deposition at relatively low temperature and atmospheric pressure.

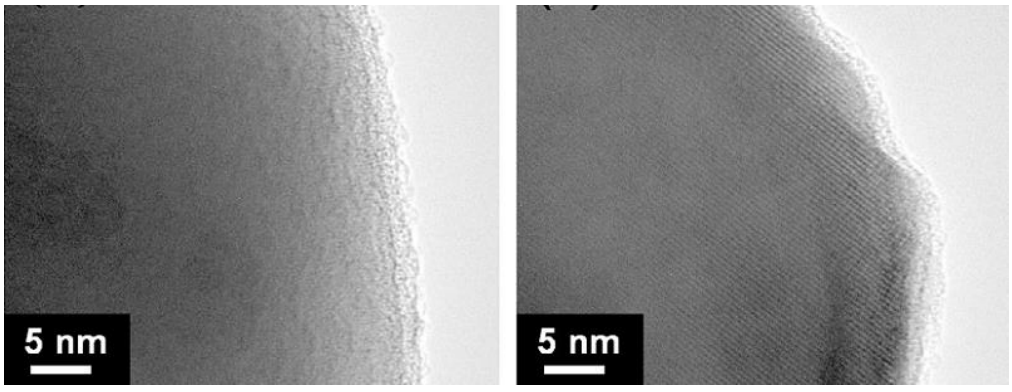

Figure 1-7 HRTEM images of Conformal SiO_2 ALD films on (left) anatase and (right) rutile pigment TiO_2 substrates. [21]

TiO_2 has propensity to photodegrade organic-based substance in the vicinity of the surface as a commonly used photocatalyst because of the free radical generation under UV irradiation. On the one hand, for commercial application, usually in white pigment industry, suppression of inorganic insulating thin film is desired to quench the photocatalytic activity of pure TiO_2, on the other hand, multi-layer of SiO_2 and TiO_2 is reported that can enhance the photocatalytic

activity of pure titania. Weighing all the pros and cons of different synthesis methods including wet chemical process (i.e. sol-gel) and gas phase-based process (i.e. CVD and FBR-ALD), liquid based process is less than ideal since impurities stays in the substrate and the bad stability when washing or separation etc. in industrial applications. Compared with different gas phase-based methods, CVD as the most commonly used method delivers all the precursors into the reactor simultaneously which further will make the film non-conformal, porous and isolated islands on the surface that reduce lifespan of silica coated TiO_2 particles to a great extent. It is really tough to control the tortuosity of pores for pinhole-laden SiO_2 thin films by CVD. In other words, the quality of CVD-SiO_2 thin layer is not controllable perhaps. During pigment batches, neither sol-gel method nor CVD process handle the growth of thin film precisely. Furthermore, ALD process can overcome these shortcomings mentioned above to achieve precise thickness control and conformal morphology.

1.3 Deposition of SiO_2 on TiO_2

As the most commonly used white pigment, TiO_2 has lots of pros like high refractive index and photostability. However, high photocatalytic activity makes degradation easier than other white pigments. [6] Hence, core-shell structure of SiO_2 deposited on TiO_2 may do help to eliminate such a high photocatalytic activity. Precursors used are silicon tetrachloride and water. Roger et al. worked on the surface composition of titania particles by TGA as shown in Figure 1.9.

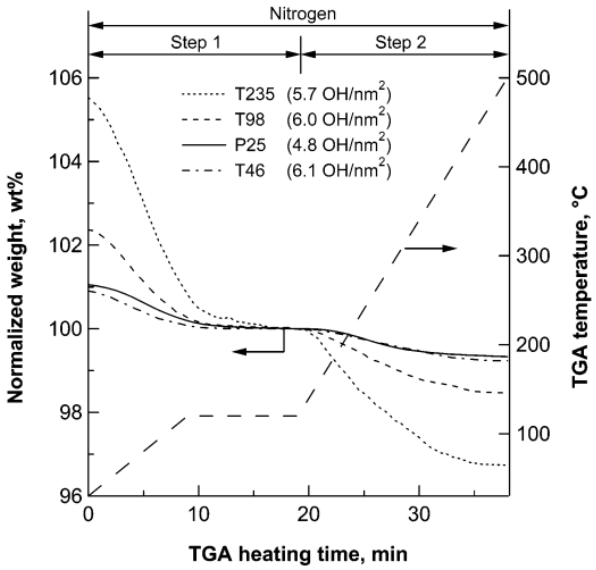

Figure 1-8 TGA graph of pure fumed titania (T235, T98 and T46) which indicate the surface areas of 235,98 and 45 m^2/g, respectively, and commercial fumed titannia P25[5].

The physically absorbed water and chemically bonded water (always -OH group in principle)

could be distinguished in Step 1 and Step 2 respectively via these three dash lines of pure titania particle. The first plateau means the temporary stable state except the physically absorbed water while the last plateau tells the final stable state at high temperature, 500°C, where the chemically bound water is evaporated.

The reaction of depositing silica on titania can be divided into two containing the two pulsing processes of different precursors ($SiCl_4$ and water). Total reaction is described as: [7]

$$SiCl_4 + 2H_2O \rightarrow SiO_2 + 4HCl \quad (1.2)$$

For ALD process, the first and second part of self-limiting reaction are: [8]

$$|-OH(s) + SiCl_4(g) \rightarrow |-O-Si-Cl(s) + HCl(g) \quad (1.3)$$

$$|-O-Si-Cl(s) + H_2O(g) \rightarrow |-O-Si-OH(s) + HCl(g) \quad (1.4)$$

where |– OH(s) and |–Si – Cl(s) represent the surface hydroxyl and chlorosilicon groups, respectively. Till now, one complete cycle is finished. When the samples are prepared, through photodegradation of Rhodamine B mixed with powders, the photocatalytic activity is measured.

The coverage of SiO_2 sub-monolayer is ascribed to steric hindrance between adjacent precursor molecules that lead to a sparse nucleation site pattern. $SiCl_4$-based processes yield higher growth rates on nanoparticles due to the significantly smaller molecular size, low evaporation temperature and pressure, which would lower the dozing time required to deposit a thick suppressing film. The main purpose of silicon dioxide application by ALD is about its optical properties. This amorphous films has an extraordinary low optical loss within a spectral range of 200nm to 1100nm. [10] The scalability of film thickness is not bad while it's optically homogeneous which allow a high accuracy of optical devices. In addition, porosity, correlating to the shift of transmittance spectra, could be suppressed by oxide films such as SiO_2 and Al_2O_3 layers.

1.4 Properties of SiO_2/TiO_2 catalysts

Based on the high chemical stability, TiO_2 is mostly ideal substance for photocatalysis and expressed as three crystalline structures: anatase, rutile and brookite, where anatase exhibits the best photocatalytic properties, however, it will change to rutile at high temperature about 900°C. Another vital merit is the excellent oxidizing effect which makes titania competitive for degradation of both organic and inorganic compounds via lowering activation energy at relatively low concentrations ranging from 0.01ppm to 10ppm. Applications about TiO_2's good photocatalytic activity can be categorized as self-cleaning, decomposition of gas pollution and etc.

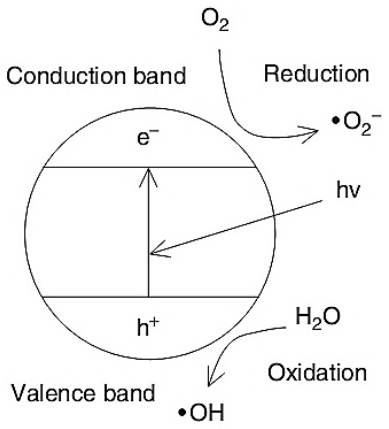

Figure 1-9 Schematic of TiO_2's Oxidation-Reduction reactions under illumination

Under illumination, the induced separation of carriers occurs by protons to generate electrons(e^-) from conduction band to valence band, leaving holes(h^+) behind in the valence band. The minimum required energy equals to energy difference of band gap(E_g) and E_g of anatase is 3.2eV, which corresponds to the photons with a wavelength of 388nm. As shown in Fig 1.10, the generated electrons are able to reduce acceptor molecule A which could be described as the equation below.

$$A + e^- \rightarrow \cdot A^- \tag{1.5}$$

Meantime the donor molecule B will be oxidized by photo-generated holes and such holes are accepted by hydroxyl group or water molecule which depends on the pH value to produce hydroxyl radical (·OH) afterwards and prevent electron-holes recombination to yield high reaction rate which further correlates with high photocatalytic activity [25]:

$$D + h^+ \rightarrow \cdot D^+ \tag{1.6}$$

$$H_2O + h^+ \rightarrow \cdot OH + H^+ \ \ or \ \ 2OH^- + h^+ \rightarrow \cdot OH + OH^- \tag{1.7}$$

Oxygen in water or air acting as electron acceptor can be reduced by generated electrons to form superoxide ion($\cdot O^-_2$) which is very reactive for oxidation of organic molecules.

$$O_2 + e^- \rightarrow \cdot O^-{}_2 \tag{1.8}$$

Normally, the dye materials commonly used are Rhodamine B. Feng Chen et al. studied the degradation processes of TiO_2 and TiO_2/SiO_2 in Rhodamine B solution with pH~4.3. The different mechanism at different irradiations are as followed. 1). Under visible irradiation, photon absorption of RhB enables the transferring of LUMO electrons from RhB molecules to the conduction band of TiO_2 which reacts with oxygen to produce active oxygen species. 2). Under UV irradiation, photon absorption of TiO_2 plays major role which further reacts with H_2O, O_2 and −OH group to produce active oxygen species. In this case, the effects of adsorption of RhB is relatively vital for photodegradation under visible irradiation. Furthermore, in the first case, they observed for the adsorption groups of RhB, the ring cleavage for the carboxyl adsorption and deethylation for alkylamine adsorption when the active oxygen species

attacked the organic groups nearby. It must be noted that there is a fast dynamic adsorption/desorption equilibrium of RhB and its deethylated species between the solution bulk and the TiO_2 particle surface during the photocatalytic deethylation stepwise process of RhB (as shown in Fig 1.11).

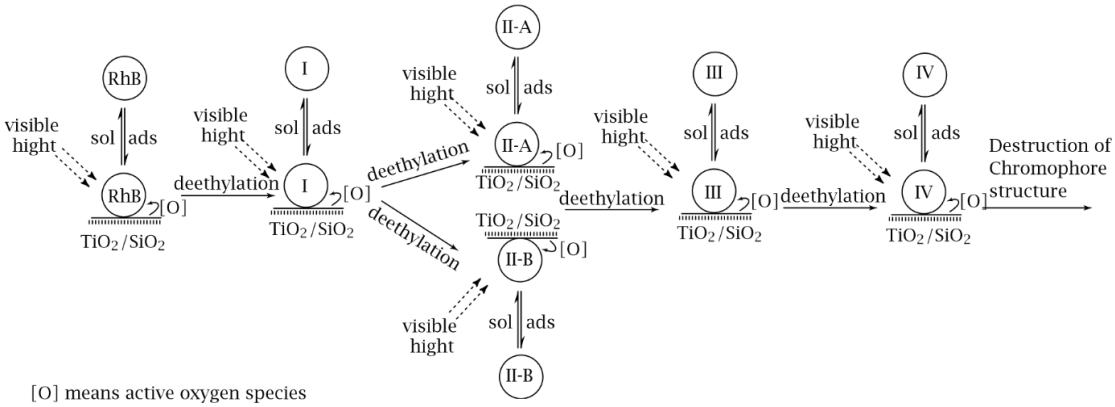

Figure 1-10 Schematic of stepwise deethylation process and the dynamic equilibrium of RhB and its deethylation intermediates species between the surface of TiO_2/SiO_2 and bulk solution in the photocatalytic oxidation of RhB.

In the second case, the adsorption of dye materials is minor factor for photodegradation process. Thus, for the carboxyl group adsorption, the chromophore structure of RhB was preferentially degraded directly with active oxygen species under both UV and visible light irradiation while for the diethylamino group adsorption, RhB would prefer to be deethylated by the active oxygen species under visible light irradiation.

Suppression of SiO_2 coated TiO_2 nanoparticles by sol-gel method has been studied by H. S. Lee et al. One of the reasons is the interface between SiO_2 and TiO_2 nanoparticle which is characterized by FT-IR and Si-O-Ti bond by XPS and such bond broaden the band gap. Another reason is that the thick silica thin film block most of the active sites which further hinders the production of active oxygen species. [26] Another addictive advantage of Si-O-Ti bond in SiO_2/TiO_2 interface is the stabilization of crystallite transformation from anatase to rutile and the transformation temperature is 700°C for Degussa P25 TiO_2 nanoparticles, [27] a benchmarking photocatalyst. The formation of rutile by calcination can reduce the surface-adsorbed water and hydroxyl groups and specific surface area to lower photocatalytic activity.

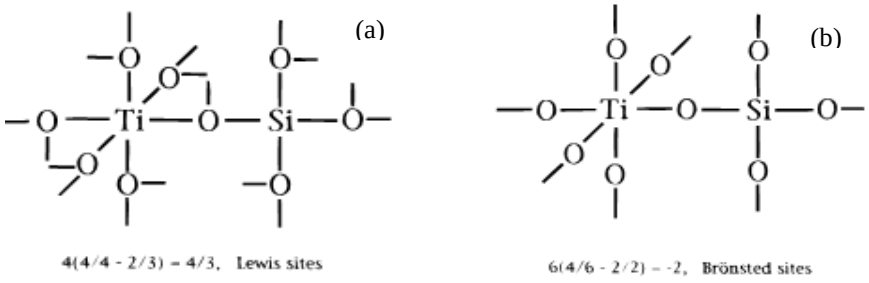

Figure 1-11 Illustration of Si-O-Ti linkage a) Lewis sites and b) Bronsted sites [30]

Wu et al. proposed a multilayer structure of silica and titania thin films by ALD. [28] The

interface which is much thinner than that of suppression between two different layers also forms crosslinking of Si-O-Ti bonds, thus decrease the positive charge of Ti atoms in the interface. There are two models built by Tanabe et al. to explain the enhancement.

TiO_2 is octahedrally coordinated with oxygen which is bonded to 2 Si atoms and Ti ion enters the lattice of SiO_2 with the same coordination number, since the Ti ions are still bonded to the same number of oxygens with different coordination number. In this case, the charge imbalance is created which is negative. As shown in Figure 1.12 a), Lewis sites match the lattice of interface if the charge is positive while the imbalance is calculated by integration of every contribution of individual contribution. Extra protons can be found in Bronsted sites when the charge imbalance is negative which is calculated in the same manner of Lewis sites. 4 valence electrons of Ti ion divided by 6 bonds of oxygen atom minus two free electrons of oxygen which provide the charge imbalance as -1/3 per bond. More surface hydroxyl groups are expected since the negative imbalance attracts more protons with the nearby oxygen atoms. The different physical crosslinking model of lattice substitution is based on the different Si/Ti content ratio. Doolin et al. reported Bronsted sites are preferential with less content of silica and vice versa. [31] Besides the Si-O-Ti bonds charge effect, it also reduces the mobility of electrons in TiO_2 phase and polarizability of oxygen atoms which prevents the rapid recombination of carriers at the interface. [29] Another mechanism is that the TiO_2 behaves as the photoactive center of the TiO_2/SiO_2 multilayer, e.g., generating hydroxyl radicals under irradiation, in the same time, the SiO_2 phase provides better adsorption sites in the vicinity of the TiO_2. [32]

Different fabrication methods of SiO_2/TiO_2 core-shell or multilayer structure effect on the photocatalytic properties both of suppression and enhancement. Atomic layer deposition provides the most conformal film and precise control of film growth. Nonporous conformal relatively thick layer has the best passivation of photocatalytic activity as mentioned above which could be got via ALD. For enhancement of multilayer structure, sol-gel cannot enable this phenomenon while ALD-silica/titania structure is more stable and conformal than CVD.

In this work, we demonstrate a conformal thin film of SiO_2 on TiO_2 nanoparticles via atomic layer deposition (ALD) with $SiCl_4$ and H_2O. The saturation state of dosing $SiCl_4$ is investigated by varying the time of pulsing. The operating temperature of ALD-FBR can be lowered to room temperature at atmospheric pressure which is much lower than that of $SiCl_4/H_2O$ thermal ALD. By varying the thickness of silica thin film, the photocatalytic activity can be tuned from suppression to enhancement that is measured by UV-vis analyses after UV irradiation with a relatively low GPC about 0.7 Å. The most important factor of photocatalytic enhancement is the presence of Si-O-Ti bonds in the interface which can be characterized by XPS and FT-IR. The optical absorption of the interface indicates the energy difference of band gap. In addition, annealing also enhanced the photocatalytic properties of such materials with core-shell structure to a certain extent.

Chapter II

2. Experimental Section

2.1 Experimental Set-up

Experiments are carried out in a fluidized bed reactor are described by David et al. [33], which is composed by a vertical glass column of 26 mm internal diameter and 500 mm height, placed on a single motor Paja PTL 40/40-24 vertical vibration table to assist the fluidization. The vibration table is operated at 35 Hz, and provides a vibration amplitude of 2 mm to the column.

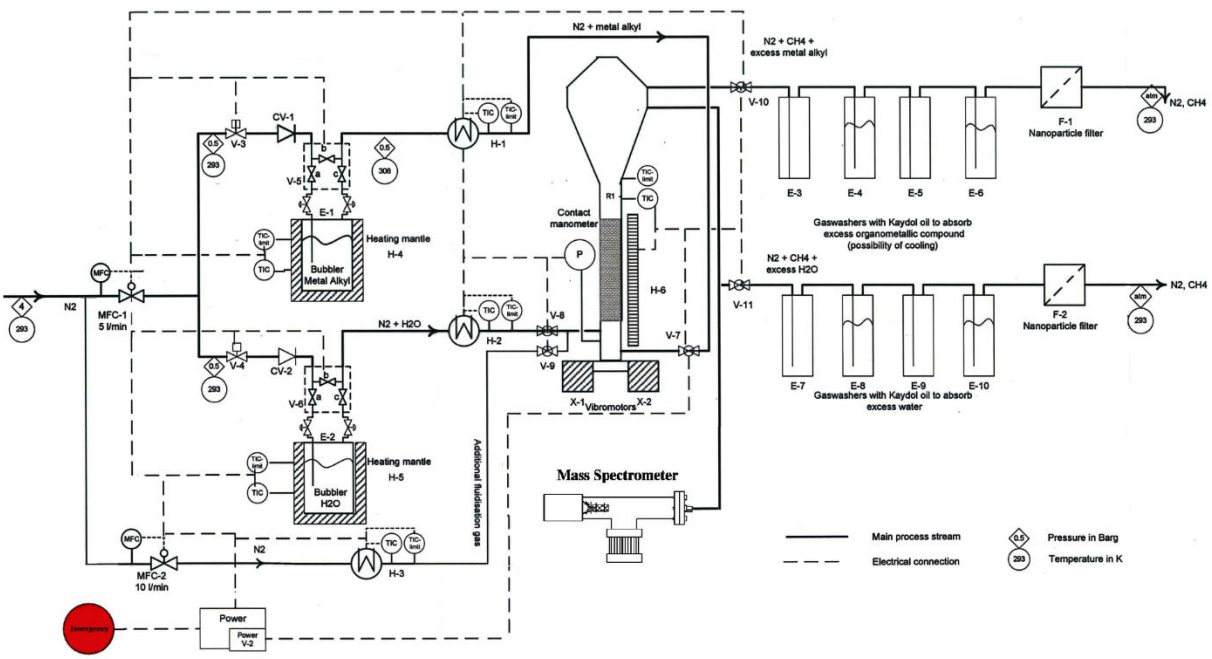

Figure 2-1 Set-up of Atomic Layer Deposition in Fludized Bed Reactor (The detailed parts can be found in Table 1 of Appendix A)

An infrared lamp placed parallel to the column, and a type-K thermocouple inserted in the column, are used to control the bed temperature with a tiny fluctuation (±5°C). The gas is introduced to the column through a stainless-steel SIKA-R 20 AX distributor plate of sintered particles with a pore size of 37 µm, to achieve a homogenous flow of gas through

the full cross-section of the column. An identical distributor plate is placed on top of the column twined around cylindrical surface by Teflon tape to prevent nanoparticles from leaving the column. Although the pore size of the distributor plates is several orders of magnitude larger than the particle size, the risk of losing particles is small since they do not fluidize as individual particles, but as agglomerates of 200–300 μm. These agglomerates, which have a void fraction of 98%–99%, demonstrate a dynamic behavior during fluidization. [34] This means that the agglomerates break and recombine constantly as a consequence of the collisions between solids. The dynamic behavior and large porosity of the agglomerates ensure that the precursor molecules reach the whole surface area of the individual particles, even though they exist as agglomerates.

Degussa P25 TiO_2 with the mean diameter about 21nm and specific surface area of approximately 54m^2g^{-1} measured by BET method (Brunauer–Emmett–Teller) were supplied by Evonik Industries (Hanau, Germany). Silicon tetrachloride ($SiCl_4$) was provided by Akzo Nobel HPMO (Amersfoort, the Netherlands) and the second precursor was deionized water vapor. Both of these two precursors were kept in stainless steel bubbler while the former is 500ml and the latter is 150ml. Pressurized nitrogen (99.99 vol.%) was used as the carrier gas. A flow of nitrogen which is 0.5L/min is applied to fluidize the powder and carry precursors.

2.2 Design of the Experiment

To calculate the precursor dosing times, we estimated the total amount of active sites in the bed of particles, i.e., hydroxyl groups. This amount is calculated with the surface area of the Degussa TiO_2 (54 m^2/g), the mass of powder placed inside the column (1.5 g), and the surface concentration of hydroxyl groups (3.3 OH/nm^2) [35]. Furthermore, we can get the initial amount of OH groups which is 4.44×10^{-4} mol. $SiCl_4$ is easy to be evaporated hence we didn't heat the bubbler containing $SiCl_4$ which means kept it at room temperature (~27°C). According to the ideal gas law, the amount of evaporated $SiCl_4$ can be calculated via the equation below as 13.95 mol m^{-3}.

$$C = \frac{n}{V} = \frac{P}{RT} \tag{2.1}$$

where P is the vapor pressure, R is the ideal gas constant as 8.314 Pa m^{-3} mol^{-1} k^{-1} and T is the operating temperature of bubbler. Vapor pressure of $SiCl_4$ at 27 °C calculated by August equation is 3.48kPa. The nitrogen flow we used is 0.5 L/min and assuming all of the sent $SiCl_4$ are reacted with the active sites of P25 TiO_2 nanoparticles. Estimation about dosing saturated time of $SiCl_4$ can be given by amount of OH groups divided by the amount of evaporated $SiCl_4$ times nitrogen flow. The saturating dosing time of first precursor is about 3.82 seconds but the assumption is quite ideal and not all of the molecule of SiO_4 will react with OH groups. So, the dosing time of $SiCl_4$ we used varied from 5 seconds to 1 minute (5s, 10s, 20s, 40s and 1m). Moreover, the purging time after pulsing of $SiCl_4$ is 3 minutes while it is 8 minutes after second

pulsing of deionized water vapor and the dosing time of oxidizer is 3 minutes. Briefly, the feeding sequence is 1min/ 3min/ 3min/ 8min. Operating temperature is varied from room temperature (~27°C) to 250°C (RT, 100°C, 200°C and 250°C). The substrate temperature must be high enough to prevent condensation of any of the reactants. If condensation occurs during an ALD cycle, undesirable or uncontrollable reactions might happen, resulting in the formation of porous and impure films. However, an undesirable decomposition of a reactant will happen if the temperature is too high . Furthermore, CVD reactions will start to occur, which leads to an uncontrolled deposition of the film. Moreover, different number of cycles influences the thickness of SiO_2 thin film directly with 2, 5, 8, 10, 12, 20, 30 and 40 cycles. In addition, the effects of annealing for SiO_2 coated TiO_2 nanoparticles on photocatalytic activity is also studied.

2.3 Characterization of Nanoparticles

As-coated SiO_2/TiO_2 powders were suspended in ethanol and transferred to regular transmission electron microscopy (TEM) grids (3.05 mm in diameter). TEM images were taken at several locations on the grids using a JEOL JEM 1400 transmission electron microscope operating at a voltage of 120 kV and a current density of 50 pA cm^{-2}.

X-ray photoelectron (XPS) characterizations were carried out using a ThermoFisher K-Alpha system using Al Kα radiation with photon energy of 1486.7 eV. A sufficient amount of powders was immobilized on carbon tape before loading into the XPS chamber. Survey scans were acquired using a 200 µm spot size, 55 eV pass energy and 0.1 eV/step with charge neutralization. The peaks positions were calibrated according to the C 1*s* peak at 284.8 eV.

The SiO_2/TiO_2 powders were transferred onto a Si wafer with 300 nm of SiO_2 thermally grown amorphous oxide. This was to eliminate the influence of the substrate (Si) signal in the XRD patterns of the powders. XRD patterns were obtained by a PANalytical X-pert Pro diffractometer with Cu Kα radiation, secondary flat crystal monochromator and X'celerator RTMS Detector system. The angle of interest 2θ was measured from 10° to 90° with fine steps of 0.001°.

The specific surface area (SSA) of the powders was determined by performing N_2 physisorption on a Micromeritics Tristar II at 77 K. For each measurement, 160 mg of the powders was used. All the samples were annealed in N_2 at 150 °C for 16 hours prior to the measurements. Data analysis was performed using Microactive software V3.02. The BET SSA was determined by fitting of data points in the P/P_0 = 0.05-0.225 region. The microporous volume and external surface area were determined by the t-method, obtaining a linear fit in the De Boer thickness of more than 15 data points [61].

A Mettler Toledo TGA/SDTA 85le thermogravimetric analyzer was used for studying the thermal behavior of the synthesized powders. An amount of approximately 10 mg of powders

was used for each TGA measurement. The TGA curves were recorded while (1) heating up the powders from 25 to Ti = 120 °C with a ramping rate of 10 °C min^{-1} in a N_2 flow of 100 mL min^{-1}; (2) maintaining at 120 °C for 10 min; (3) ramping up to 550 °C with a ramping rate of 20 °C min^{-1}; and (4) finally maintaining at this temperature for 10 min. Steps (1) and (3) are commonly used to determine the density of physisorbed water and chemisorbed hydroxyl groups on the surface, respectively [62].

Optical absorption measurements were performed using a PerkinElmer-Lambda 900 spectrometer equipped with an integrated sphere device. The powder was suspended in ethanol, which was transferred onto a quartz substrate and dried in atmosphere. The spectra were acquired in the wavelength range of 600-200 nm, with fine steps of 1 nm.

The atomic concentration of the deposited SiO_2 was determined using neutron activation analysis (NAA), which was carried out at Reactor Institute of Delft (Delft University of Technology). The powders (about 100 mg for each sample) were loaded into high purity polyethylene capsules. The samples and a standard sample (reference) were then packaged and irradiated in a suitable reactor at a constant neutron flux. All reactors used for neutron activation employed uranium fission, which provides a neutron flux in the order of 10^{12} cm^{-2}. These neutrons have low kinetic energy, typically less than 0.5 eV. Upon irradiation, a neutron can be absorbed by the target nucleus (i.e. Si), forming a radioactive nucleus, which carries its own half-life characteristics. The nuclear decay of the radioactive nuclei produce gamma-rays, which are detected by the NAA detectors, from which the Si loading was determined. For SiO_2/TiO_2 samples, the waiting time of 5 days was applied during the decay of radioactive nuclei. For Si, the NAA used in this work allows to detect at the level in the range of 10^1-10^2 nanogram.

The photocatalytic activity of the SiO_2/TiO_2 powders was evaluated by the photodegradation of RhB solution. For each test, 30 mg of the powders were added to 30 mL RhB solution (concentration of 8 mg L^{-1}) and continuously stirred in the dark for 30 min to obtain a uniform suspension. Thereafter, the suspension was exposed to UV radiation generated by a mercury lamp with a power of 45 W for different exposure times. The set-up allowed to carry out up to 10 samples simultaneously, which ensured that all samples were irradiated under the same conditions, such as light intensity, exposure time, and temperature. The suspension was then centrifuged to separate the powders from the solution. Finally, the solution was analysed by UV-visible spectrophotometry to determine the residual concentration of the RhB in solution with the wavelength from 300 nm to 800 nm where the characteristic wavelength we used is 554 nm, which was used to evaluate the photocatalytic activity of the SiO_2 layers both about suppression and enhancement.

Chapter III

3. Results and Discussion

3.1 Film Thickness and Si Concentration characterized by TEM and INAA

The self-limiting reaction of $SiCl_4/H_2O$ in ALD process demands a relatively high temperature as the driving force of ligand exchange among functional groups in the surface such as hydroxyl groups and the typical range is about 300 to 400°C which could be lowered by adding catalyst such as NH_3. [21,43] However, silicon tetrachloride is a potential material to enable the ALD process at relatively low temperature and atmospheric pressure which is attributed to its low vapor pressure at room temperature and low vapor temperature in atmosphere that is very attractive, in the one hand, for industrial applications and scaling up due to the energy-saving, safe operating conditions and stable working state and in the other hand, room temperature avoid fluctuation of operating temperatures in the reactor. In the first case, Jing et al. demonstrated an approach to run the $SiCl_4/H_2O$ system at room temperature without catalyst while accompanied with high operating pressure and partial pressure. [44] At this kind of experimental conditions, high total and partial pressure is dominant for silica nucleation and growth of silica thin films. [45] Here, we propose an atmospheric pressure ALD in fluidized bed reactor at low temperatures to grow conformal silica thin film on P25 TiO_2 nanoparticles using silicon tetrachloride and deionized water vapor. The saturation state of dosing $SiCl_4$ is studied with different pulsing time which was already calculated above at the nearly ideal circumstances from 5 seconds to 1 minute. TEM was implemented to characterize the thickness of SiO_2 ultrathin film while silicon concentration was measured by INAA as shown in Figure 3.1. As for the silicon concentration with different $SiCl_4$ dosing time indicated in Fig. 3.1 (g), the same amount of silicon products was found for 5 seconds and 1 minute both at 100 °C and 200 °C which are approximately 2.1 at. % and 2.5 at. % respectively which means 5 seconds is enough for dosing the precursor $SiCl_4$ to get saturation for self-limiting reaction. For 12 cycles, the tendency of Si concentration at different temperatures is in agreement with its of SiO_2 thin film's thickness. Here it has to be noted that the thicknesses of SiO_2 thin film at different temperatures are almost the same except at room temperature as well as the Si concentration. In other words, in such range of operating temperature (100 SiO_2 °C to 250 °C),

the growth per cycle (GPC) is independent of temperature while at room temperature, condensation will occur due to the vapor temperature of water in Fig. 3.1 (h). Despite the negligible change of GPC at different temperature, the most precise control to grow SiO_2 thin film is realized at 100 °C and Figure 3.1 (h right) shows the linear relationship between number of cycles and thickness (or Si concentration) 100 °C and the slope of linear estimation represents a small GPC (~0.8Å) with the feeding sequence of $SiCl_4/N_2/H_2O/N_2$ 1/3/3/8 (minute).

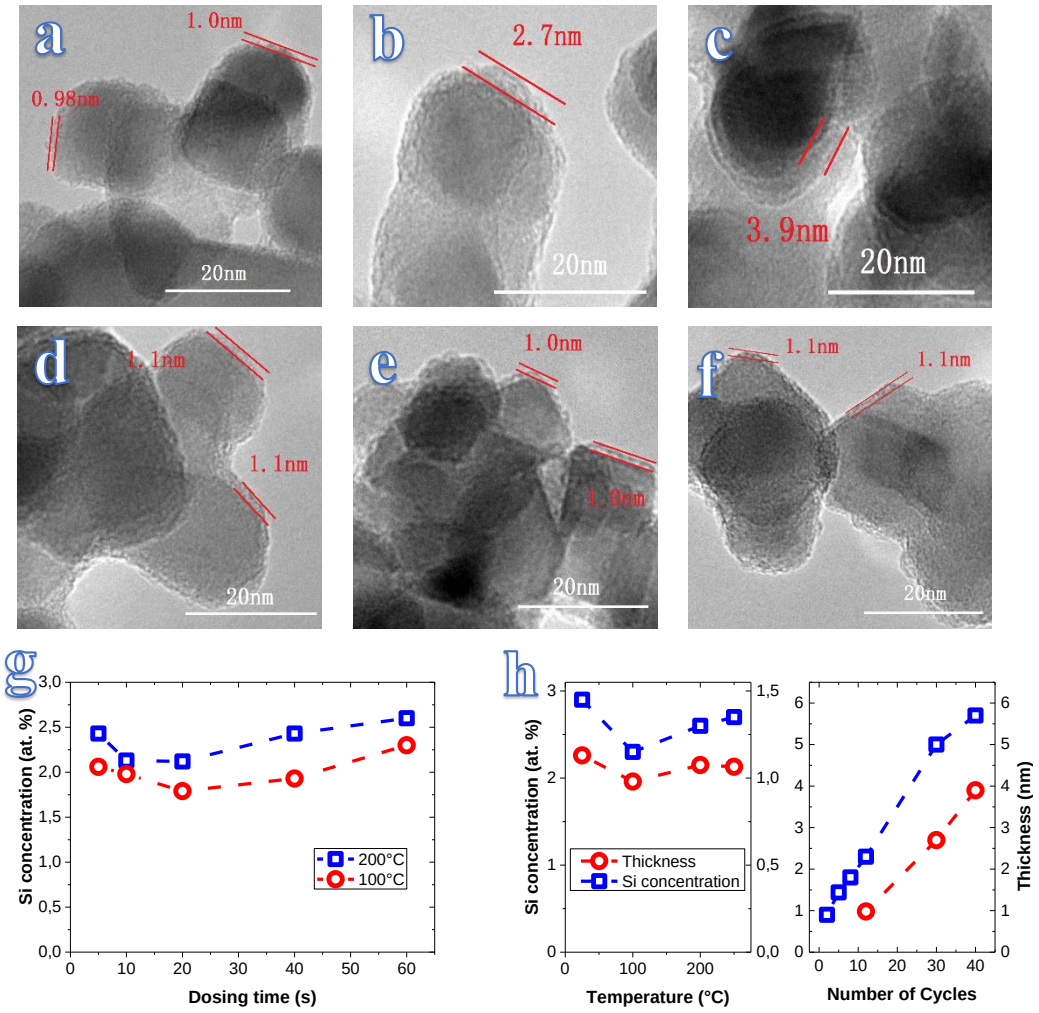

Figure 3-1 Representative TEM images of the TiO_2 NPs coated with SiO_2 grown for (a) 12 cycles, (b) 30 cycles, and (c) 40 cycles at 100 °C, and for 12 cycles at (d) room temperature, (e) 200 °C and (f) 250 °C. The plot of Si concentration as vs dosing time of $SiCl_4$ at 100 °C and 200 °C is shown in (g). The left of (h) shows the plot of temperature vs Si concentration and thickness for 12 cycles and right of (h) indicates the function of number of cycles vs Si concentration and thickness at 100 °C).

Here, the specific surface area (SSA) of P25 TiO_2 nanopowders we used for the calculation of dosing time in the *Experimental Section* was determined by N_2 physisorption isotherm as well as the pore volume of the coating layer. For uncoated P25 TiO_2 nanoparticles, the SSA is 54.5 m^2g^{-1}. The plot demonstrates a trend that the volume of micropores and SSA would increase

with the increasing of number of cycles although a slight fluctuation of total SSA was found as shown in Figure 3.2 which means the external SSA was reduced. The thickness can be calculated with the approximation of SSA vs average diameter of particles as follows.

$$SSA = \frac{6}{\rho D} \tag{3.1}$$

where ρ is the density of nanopowders and D is the particle diameter. The initial particle diagram is 21 nm and density of Degussa P25 TiO_2 nanopowders is 4.26 g/mL. The increasing of thickness when increased the number of cycles in ALD process are almost in consistent with the growth of SiO_2 thin films and the agglomeration is the minor factor in this kind of ALD process.

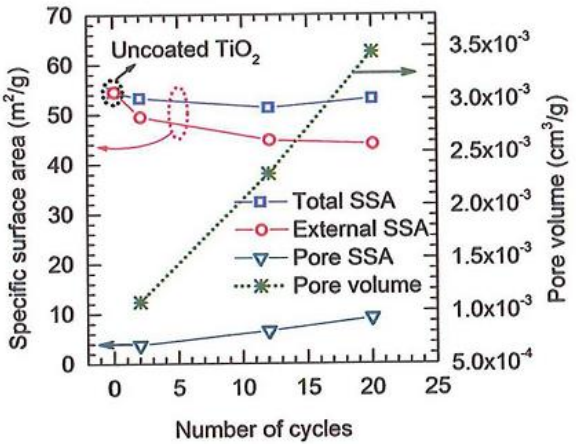

Figure 3-2 Total and external specific surface area of the uncoated TiO_2 and the TiO_2 coated with SiO_2 at 100 °C for different number of cycles.

3.2 Characterization of Composition and Interface of SiO_2 coated TiO_2

The composition of uncoated TiO_2 and SiO_2 coated TiO_2 at room temperature (~27 °C), 100 °C and 200 °C are characterized by XPS which can be seen in Figure 3.3. The binding energies (BE) of the elements were calibrated by referencing the C-C peak of C 1s to 284.8 eV (Figure 3.3a-d) [48]. In the region of Si 2p and O 1s, the Si 2p peak at 103 eV (Figure 3.3 e-h) in conjunction with the O 1s peak at 532.5-532.7 eV which was designated as O_{-Si} afterwards in Figure 3.3 i-l correspond to the Si-O coordination [53]. For stoichiometric SiO_2, a BE difference *(ΔBE)* between O_{-Si} and Si 2p of 429.3-429.4 eV is expected [53]. In this work, *ΔBE* was found to be in the range of 429.5-429.7 eV that slightly differed in deposition temperature. The higher *ΔBE* indicates the formation of nonstoichiometric SiO_x films ($x < 2$), which can be expected for ultrathin coating layers with a thickness of about 1 nm as measured by TEM in Figure 3.l a, d, e and f. For instance, *ΔBE* = 429.5 eV represents a nonstoichiometric SiO_x with $x = 1.6$ [54]. The intense peak around 530 eV of the O 1s spectra which was designated as O_{-Ti} afterwards in Figure 3.3 i-l and the peak around 458.8 eV of the Ti 2p spectra (Figure 3.3 m-p) stand for the

fingerprints of Ti-O bonds of the P25 TiO_2 support [47]. Noticeably, there was one remarkable shift towards higher binding energy of both the $O\text{-}_{Ti}$ of the O 1s and the Ti 2p peaks of the SiO_2-coated TiO_2 compared with uncoated TiO_2, which is evidence of the formation of Si-O-Ti crosslinkage (i.e., interfacial layers). [21, 47] Furthermore, for the $O\text{-}_{Ti}$ peak, a shift of 0.4eV, 0.5 and 0.6 eV was observed for the SiO_2/TiO_2 deposited at room temperature, 100 °C and 200 °C, respectively, whereas for the Ti 2p peak, the corresponding shift is 0.2eV, 0.4 eV and 0.6 eV. Accordingly, the shift is caused by the difference in charge imbalance which is explained in the *Introduction Section* between Si (~1.8) and Ti (~1.5) [55, 56]. The formation of Si-O-Ti bonds attracts more cations owing to the negative charge imbalance which induced

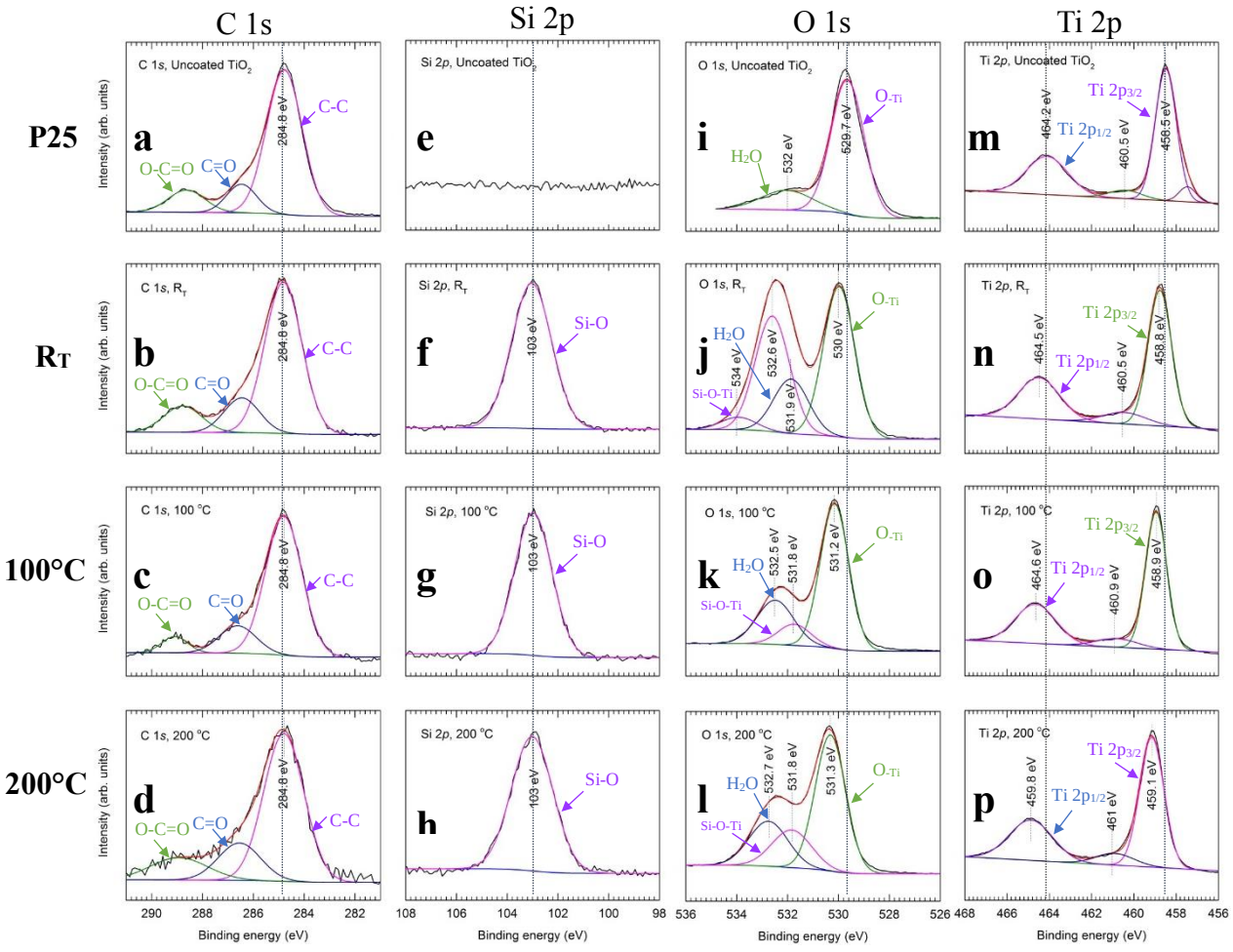

Figure 3-3 XPS spectra of bare TiO_2 and the TiO_2 coated with SiO_2 at room temperature, 100 °C and 200 °C. The binding energies are calibrated by referencing the C 1s peak to BE=284.8 eV (a-d). From left to right: C 1s, Si 2p, O 1s and Ti 2p; from top to bottom: Uncoated TiO_2, SiO_2-coated TiO_2 at room temperature, 100 °C and 200 °C for 12 cycles.

drop of the electron density around the Ti atom. This consequently increases the effective positive charge on the Ti atom, and therefore the binding energies of both $O\text{-}_{Ti}$ and Ti 2p [21,

47, 51]. In addition to the shift of binding energy, the presence of the Si-O-Ti interfaces was also observed from the deconvolution of XPS spectra, indicated by the peaks at 531.8-531.9 eV of the O 1s (Figure 3.3 i-l) and 460.5-461 eV (Figure 3.3 m-p) in Ti 2p regions [6].

FT-IR spectra can also provide the information about the presence of SiO_2 and Si-O-Ti interfacial layer in Figure 3.4 (a). Hydroxyl groups which are dominant for self-limiting reaction in ALD process and absorption of dye materials as well as the photocatalytic process locating at high wavenumber and with the absorption band in the range of 3000-3700 cm^{-1} is indicated in the left of the figure. [46] At 2355 cm^{-1}, such silica coated TiO_2 presents an obvious adsorption band of carbon dioxide and this indicted that TiO_2 coated by silica ultrathin films

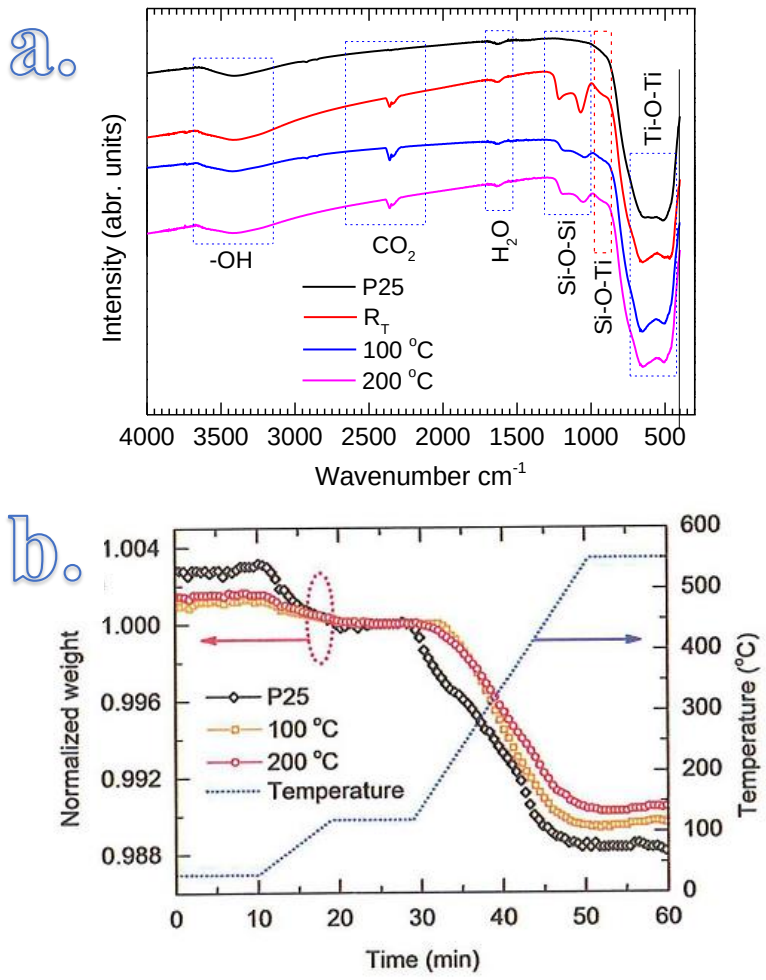

Figure 3-4 (a) FT-IR and (b) TGA diagrams of uncoated TiO_2 and the TiO_2 coated with SiO_2 layers grown for 12 cycles at room temperature, 100°C and 200 °C.

can promote the adsorption of CO_2 to a certain degree which is also reported by Yuan et al.[47] compared with uncoated ones while in the range of 1530-1710 cm^{-1}, the adsorption of water would also be seen. The presence of silica at 1000-1300 cm^{-1} showed in wavenumber is in agreement with other characterization methods. The most important thing here is the formation of Si-O-Ti interface which domains the enhancement of photocatalytic performance in a relatively narrow adsorption band and in addition, TiO_2 is also demonstrated in the FT-IR

adsorption spectra in a very wide range from 400 to 871 cm^{-1}. In the FT-IR adsorption spectra, all these three samples with different operating temperatures have significant promotion of the adsorption of CO_2 while the presence of silica shows that the one at room temperature has the most obvious amount of silica compared with 200 °C which is followed by that's at 100 °C that fits other characterizations very well. Importantly, the formation of Si-O-Ti interface at 100 °C is weaker than two others with the same order of the presence of silica. The hydroxyl groups are better demonstrated in TGA diagram as shown in Figure 3.4 (b). As for the TGA diagram, samples lost free water at 66 °C and hydroxyl bonded water at 90 °C which showed a slightly slow process than that of free water. At the last stage, hydroxyl condensation occurred which showed the chemical dehydration of the inner molecule at 130 °C for bare TiO_2 and the sample fabricated at 200°C when the one made at 100 °C is at about 200 °C. At the end, one thing should be noted that all of these three samples have less hydroxyl groups than the bared TiO_2 nanoparticles. Losing hydroxyl groups in the ALD processing of coating SiO_2 on TiO_2 particles using silicon tetrachloride and deionized water vapour as precursors is good for suppressing photocatalytic activity but bad for enhancement.

3.3 Optical Absorption Spectra and Band Gap of SiO_2 coated TiO_2

Silica thin film has a large band gap (~9eV) which will hinder the charge transfer or block the active sites for photocatalysis as mentioned above. In our work, the ultrathin SiO_2 film caused red-shift in the absorption spectra Figure 3.5 (a) and shift goes to 24nm with rising of number of cycles in ALD process for 12 cycles and then being constant. Such red-shift of absorption spectra resulted in a reduction of band gap. The band gaps can be calculated via UV-Vis spectroscopy using Tauc Plots. Here we plot the graph between $(\alpha h\nu)^2$ on y-axis and $h\nu$ on x-axis where α is the absorbance calculated from UV and $h\nu$ can be calculated by following way. $h\nu$ = 1240/wavelength. Then it's necessary to extraplot the vertical sagments of the plot to intersect on x-axis where y-axis is zero as shown in Figure 3.5 (b). That value is the band gap of our samples. Furthermore, the band gap of uncoated TiO_2 is 3.26 eV as the initial state while after two cycles' coating, the value was slightly reduced to 3.22 eV which is followed by 3.16 eV after 5 cycles. Finally, saturation state was reached after 12 cycles with the band gap as 3.10 eV. A significant difference of band gap energy between Si-O-Ti interface and TiO_2 will lead to a considerable promotion of charge transfer and excellent prevention of rapid recombination which is vital for photocatalytic enhancement.

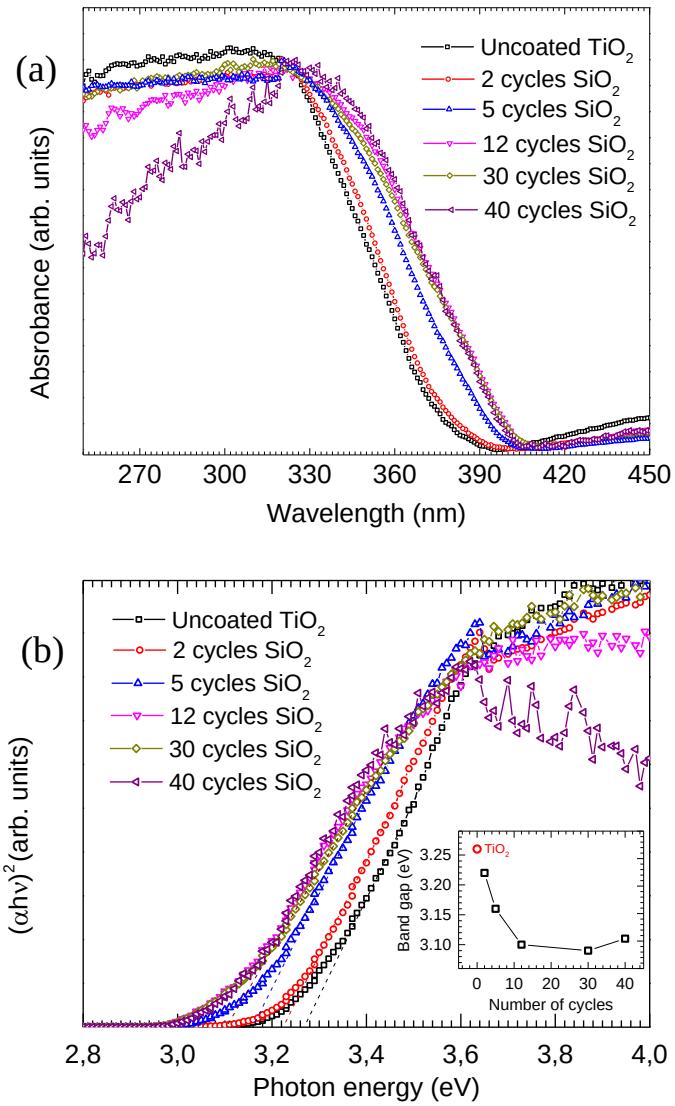

Figure 3-5 (a) Optical absorption spectra of the initial P25 TiO_2 and the TiO_2 coated with SiO_2 layers grown for different numbers of cycles and (b) the corresponding plots $(\alpha h\nu)^2$ vs photon energy ($h\nu$), from which the band gap of the material was determined. The inset of (b) shows the band gap values as a function of the number of cycles. All of the depositions were carried out at 100 °C with the pulse sequence of 1 min/3 min/3 min/8 min.

3.4 Photocatalytic Activity of SiO_2 coated TiO_2

The photocatalytic properties here emphasize more on the activity which is characterized by UV-VIS spectrometry after sunlight irradiation by a solar simulator with different intervals to get the whole photodegradation curve of RhB. In this work, an uncoated TiO_2 as the reference and blank sample without TiO_2 composited with pure RhB-dye materials are also took into consideration to compare the ability of enhancing the photocatalytic performance especially the photocatalytic activities. In Figure 3.7, the samples fabricated at different temperatures have the same trend of photodegradation corresponding to the thickness of silica thin films

and the those samples with different number of cycles in ALD process are shown in Fgiure 3.6. The

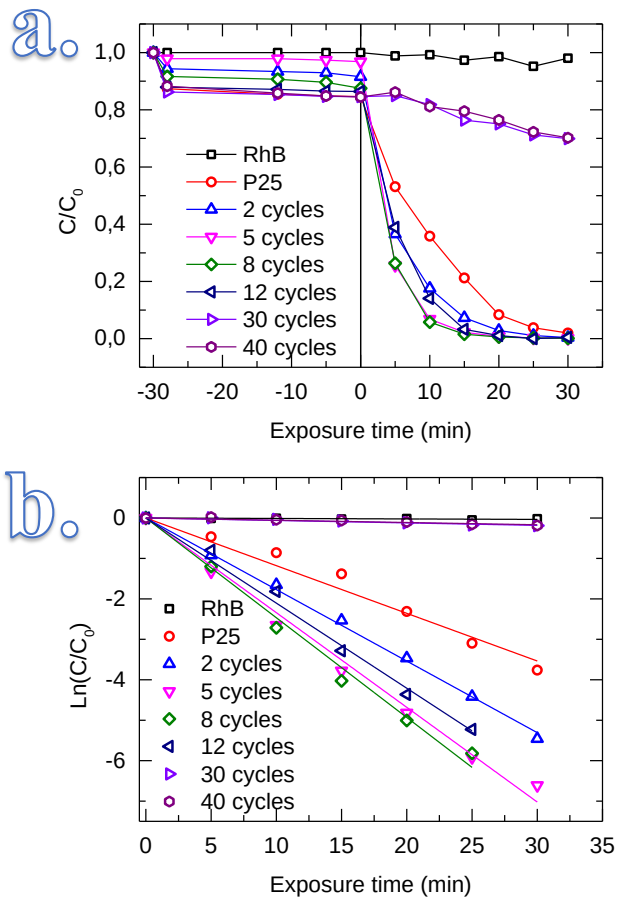

Figure 3-6 Photocatalytic activity of TiO_2 powders with or without the SiO_2 coating layers: (a) concentration as a function of exposure time, (b) kinetic plots and (c) reaction rate k_{app} as a function of the number of cycles.

threshold before UV irradiation, the solution was continuously stirred in the dark labelled as light-off stage in both of Figure 7 and 8 for 30 min to obtain adsorption/desorption equilibrium of RhB and uniform suspensions. When the irradiation begins, the critical points of every samples need to be collected every 5 minutes in order to determine the concentration of residual dye materials. In the first stage of experiment (dark environment), the RhB concentration of the blank sample (pure RhB) remained while others exhibited a small drop at the beginning due to the adsorption of RhB molecules on the surface of TiO_2 nanopowders with or without silica and then get stable very quickly. In the second stage (solar irradiation) after 40 minutes, the blank sample stayed at the same level without any TiO_2. The samples with different ALD cycles in Figure 3.6 and operating temperatures in Figure 3.7 corresponding to different thickness of silica thin films have a strong relationship between thickness and photocatalytic activities. All of the samples are decomposed completely after 40 minutes while most of the silica coated TiO_2 except the samples for 30 and 40 cycles exhibit

enhancement of photocatalytic activities.

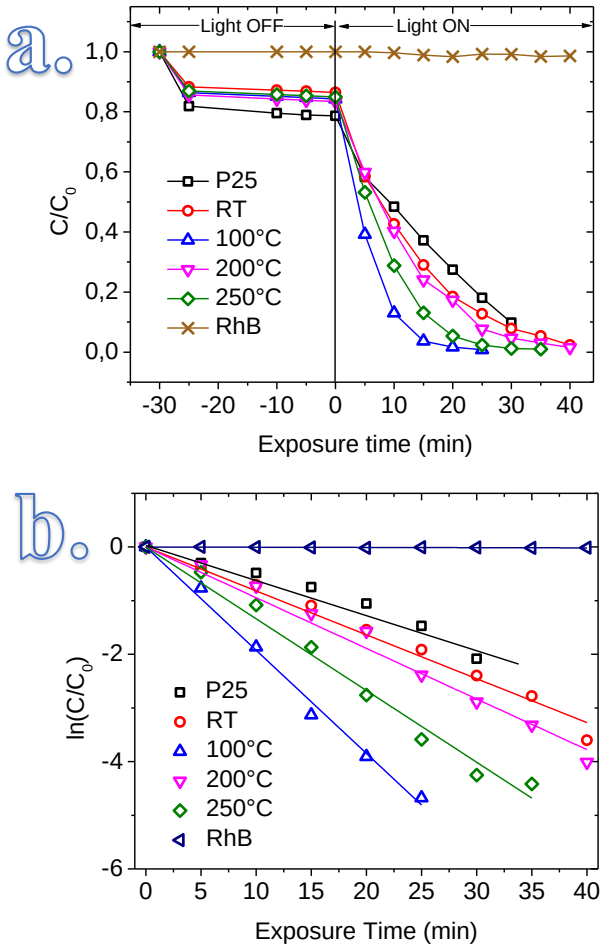

Figure 3-7 Photocatalytic activity of Rhodamine B and TiO_2 powders with or without the SiO_2 coating layers: (a) concentration as a function of exposure time and (b) kinetic plots varying the operating temperature in ALD process.

Generally speaking, the thickness-dependence can be quantitatively estimated by the kinetics of photodegradation reaction, which is described by the kinetic equation below: [49]

$$\ln\left(\frac{C_0}{C}\right) = k_{app} \times t, or \;\; C = C_0 \times \exp(-k_{app} \times t) \qquad (3.2)$$

where k_{app} is the apparent first-order kinetic constant that represents the reaction rate. The extracted plots according to the kinetic equation above are shown in Figure 3.7 (b) and 3.8 (b) with the linear estimated trendlines. The k_{app} of bare titania as reference is about 118×10^{-3} min^{-1} and others can be seen in Table 3.1. For the 40 cycles sample, k_{app} is suppressed up to 20 times and for the 8cycles' sample the photocatalytic activity is enhanced more than 2 times. Clearly here, the photodegradation is strongly dependent on the silicon thim films' thickness

coated on TiO_2 nanopowders.

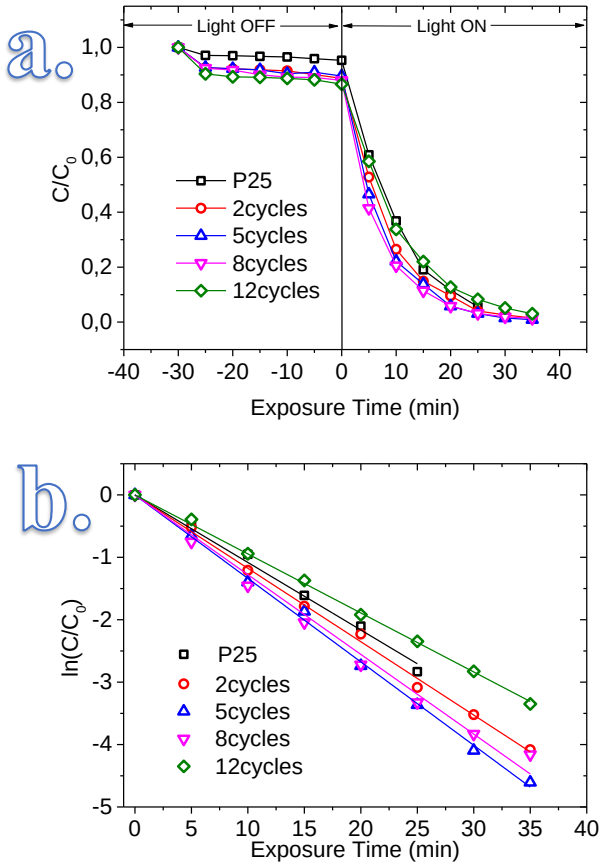

Figure 3-8 Photocatalytic activity of Bare P25 TiO_2 nanopowders and TiO_2 powders with SiO_2 coating layers deposited at room temperature: (a) concentration as a function of exposure time and (b) kinetic plots varying the number of cycles in ALD process.

Table 3-1 Apparent fist-order rate constant k_{app}, of SiO_2 coated P25 TiO_2 nanopowders under different experimental conditions.

Sample	**K_{app} ×10^{-3}/ min^{-1}**	**Samples**	**K_{app} ×10^{-3}/ min^{-1}**
Bare TiO_2	117.9	Annealed 2cycles 100°C	240.3
2 cycles at 100 °C	176.9	Annealed 5cycles 100°C	285.4
5 cycles at 100 °C	234.1	Annealed 8cycles 100°C	316.9
8 cycles at 100 °C	246.6	Annealed 12cycles 100°C	247.1
12 cycles at 100 °C	210.5	2 cycles at 27 °C	117,6
30 cycles at 100 °C	6.1	5 cycles at 27 °C	133,8
40 cycles at 100 °C	5.6	8 cycles at 27 °C	127,8
12 cycles at 200 °C	192.8	12 cycles at 27 °C	64,6
12 cycles at 250 °C	197.8	Rhodamine B	0.32

Annealing will result in the induced stress at the interface owing to different thermal expansion coefficient between TiO_2 substrate and SiO_2 ultrathin film which further change the roughness of the Si-O-Ti interface for better adsorption and provide more active sites as well as the specific surface area. [57]

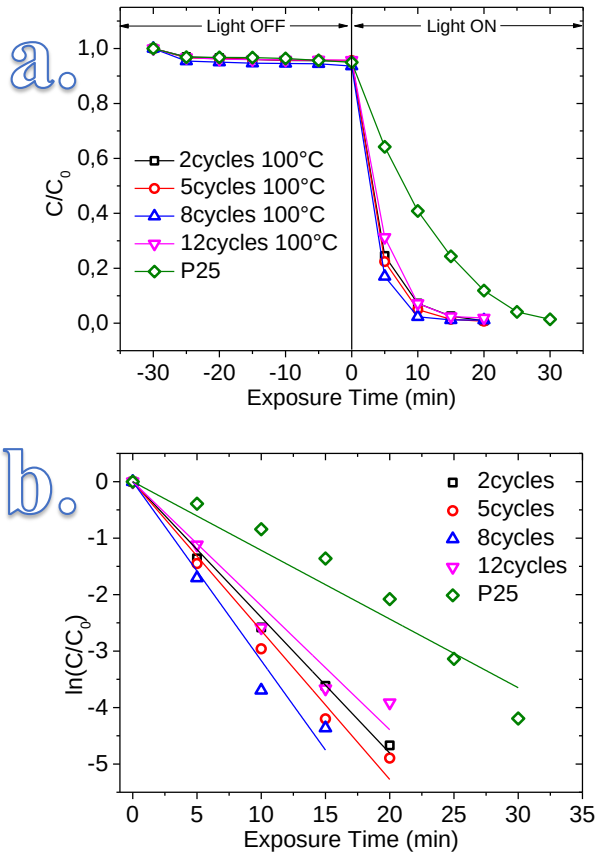

Figure 3-9 Photocatalytic activity of Bare P25 TiO_2 nanopowders and annealed TiO_2 powders with SiO_2 coating layers deposited at 100 °C: (a) concentration as a function of exposure time and (b) kinetic plots varying the number of cycles in ALD process.

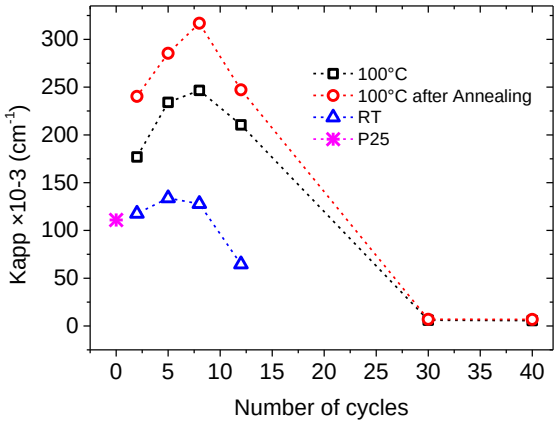

Figure 3-10 Reaction rate k_{app} as a function of number of cycles deposited at room temperature and 100 °C as well as the annealed samples deposited at 100 °C.

From Figure 3.10, it could be concluded that the sample coated at 100 °C after annealing has the best photocatalytic performance as well as other annealed samples due to the induced stress at the interface compared with the samples without annealing. The annealing was carried out in air at 450 °C for 12 hours. For the samples at 100 °C with different ALD cycles indicated that the thin film which is 7 angstroms thick supports the photocatalytic enhancement best as explained above. At room temperature, the photocatalytic enhancement is weakened to a certain extent and turns to suppression for 12 cycles as shown in Figure 3.9 even though the thickness is about 7 angstroms. When the temperature goes above 100 °C, there is a lower number of hydrogen bonded groups and an increased level of Si-O-Ti bond cleavage characterized by FT-IR with H_2O vapor addition which means the thickness of the Si-O-Ti interfacial layer cannot reach the level of other operating temperatures. [58] The growth of silica thin film begins from the initial growth of Si-O-Ti interfacial layer and then followed by the growth of SiO_2 layer which is studied by Gallas et al. [51] and the Si-O-Si bond is quite strong compared with other temperatures in FT-IR spectra while the thickness of thin film is almost the same, which in other words, the thickness of interfacial layer is smaller. Nevertheless, depositing at room temperature is still attractive due to dozens of advantages as we mentioned above. To overcome such a shortcoming of the growth of Si-O-Ti interfacial layer, many methods can be taking like using NH_3 as the catalyst may fulfil the requirement of the formation of Si-O-Ti bond cleavage. [59] Another possible reason is the quality of silica thin film due to the condensation of water vapor at room temperature resulting in a porous nature which may hinder the formation of interfacial layer. As for other samples deposited at 100 °C, 200 °C and 250 °C, they all showed peak enhancement of photocatalytic properties with a 7 Å thick thin film and the photocatalytic activities drop with the increasing of ALD cycles since the pronounced large band gap of silica block the charge transfer from both interfacial layer and TiO_2.

3.5 Mechanism of Photocatalytic Enhancement

Based on the results we got, when the silica layer on P25 TiO_2 nanopowders is lower than 1 nm, an excellent enhancement of photocatalytic performance will be realized. The presence of silica thin film promotes the adsorption of dye materials, e.g., Rhodamine B, on the surface of the nanoparticles and in the vicinity of TiO_2 sites which is proposed by Andreas et al. of the mixed SiO_2/TiO_2 system. [32, 50] But what they did is about mixing these two compounds while some of the TiO_2 are still contact with the environment, e.g., air or solution, just like the partially coated TiO_2 by SiO_2. According to the presence of Si-O-Ti interfacial layer characterized by XPS and FT-IR and red-shift measured by optical absorption analysis, we come up with another mechanism to provide better explanation based on the role of Si-O-Ti interfacial layer. Gallas et al. reported the Si-O-Ti interfacial layer can be several angstroms to one nanometer thick which is dependent to the surface morphology. [51] And small amount of silicon atoms act as dopants entering the TiO_2 lattice and create sub energy level in favour of lowering band gap to 0.2 eV [52] and this is proved by our experiment mentioned above. In the photocatalytic process, after irradiation, the photons from sunlight will generate electron from conduction band to valence band both in the Si-O-Ti interfacial layer and TiO_2 due to the comparable band gap while silica can be omitted since the band gap is quite large which means it is almost transparent to sunlight. However, the Fermi level in SiO_2 coated TiO_2 remains uncertain which means there are two models to explain the mechanisms of photocatalytic enhancement as shown in Figure 3.11.

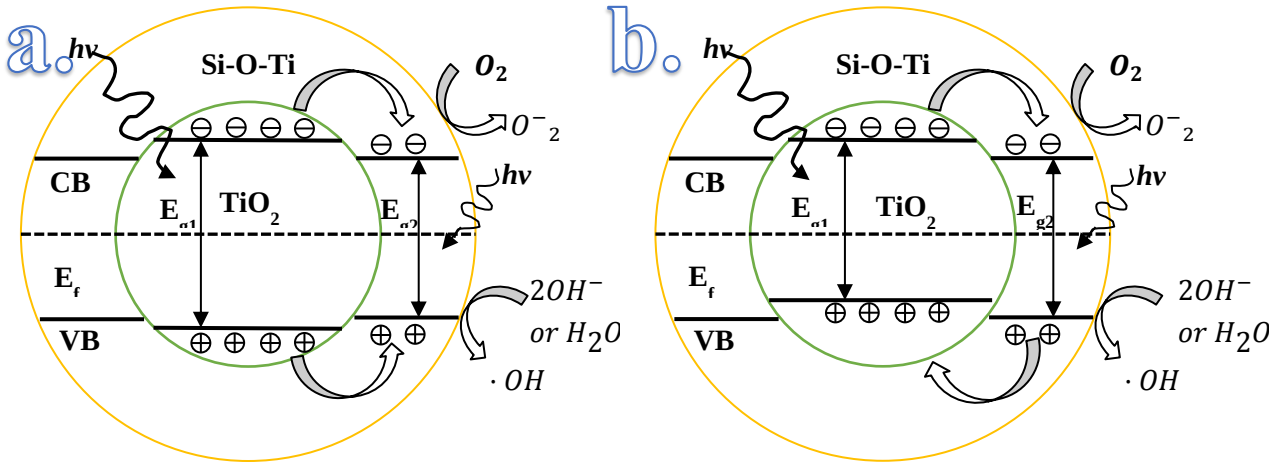

Figure 3-11 Schematics of enhancement of photocatalytic properties in SiO_2 coated TiO_2 nanoparticles. During the photocatalytic process, (a) represents the electronic structure when the Fermi levels of these two materials are the same and (b) represents the electronic structure when Fermi levels of these two are different. Both of these two diagrams includes the photon absorption in the Si-O-Ti interfacial layer and TiO_2 cores, charge transfer, recombination of carriers, production of oxygen superoxide ion and the formation of hydroxyl radical.

In the first case, Fermi level of Si-O-Ti interfacial layer and TiO_2 are almost the same which means the valence band maximum (VBM) of TiO_2 is lower than that of interfacial layer and conduction band minimum (CBM) is opposite. Because of the lower energy level in the interfacial layer, the excited electrons in conduction band and holes in valence band of TiO_2 will migrate to the interfacial layer and this charge transfer supply sufficient generated carriers, e.g., electrons and holes, to produce oxygen superoxide ion at the conduction band and hydroxyl radicals at the valence band in the interfacial layer. The formation of oxygen superoxide ion and hydroxyl radicals enables the degradation of dye materials-Rhodamine B which is demonstrated in Figure 1.11. Such charge transfer avoids the rapid recombination of carriers in TiO_2 in turn owing to the relatively low concentration. In the second case, Fermi level of Si-O-Ti interfacial layer and TiO_2 are significantly different as both of the VBM and CBM of Si-O-Ti interfacial layer are lower or higher than those of TiO_2. The former is shown in Figure 3.8 (b), the excited electrons in TiO_2 will move to the interfacial layer which is driving by the lower energy of CBM of the interfacial layer and the generated holes in the interfacial layer will migrate to TiO_2 in which leading to the fast hole trapping and then excited electrons have time to reduct oxygen to superoxide ion, meanwhile, the charge separation occurs that prevent the rapid recombination at both sides. In this way, the efficiency of photocatalysis can be improved. For the latter one, in the same manner, it induces the fast electron trapping and generated holes have time to oxidize -OH groups or H_2O to form hydroxyl radicals which could enhance the photodegradation while the electron-hole recombination is avoided, finally the efficiency is improved. If the thickness of thin film increased to a critical value, the enhancement will become weaker and finally converted to suppression because the insulating nature of silica would block the active sites at the surface around the interfacial layer and weaken the charge transfer. After 8 cycles or the thickness is lower than 0.7 nm, the enhancement becomes weaker and weaker and finally transferred to suppression for 30 cycles.

Chapter IV

Conclusions and Recommendations

4.1 Conclusions

Atmospheric pressure atomic layer deposition in fluidized bed reactor using silicon tetrachloride and deionized water vapor can be used to deposit SiO_2 ultrathin film on Degussa P25 TiO_2 nanoparticles at the temperature which can be lowered to room temperature (~27°C). The growth of thin films in almost independent of operating temperature in the range from 100 °C to 250 °C while at room temperature the condensation of water vapor caused a highest GPC in the comparison with others. The saturating state of feeding $SiCl_4$ is achieved for 5 seconds of pulsing that is evidenced by TEM and INAA to measure the thickness of thin film and Si concentration. The relatively low GPC (~0.8 Å) enables the precise control of growing SiO_2 thin film which further is able to investigate the dependence of thickness and photocatalytic activity. Another study of the deposition operating at room temperature which is very attractive in the field of industrial application and scaling up fits the trend at other temperatures with the largest GPC. Moreover, annealing is such a method that could enhance the photocatalytic properties based on the induced stress at the interface by changing the roughness. The peak value of photocatalytic activity is about 0.7 nm thick thin film and then the k_{app} value decreases to suppression eventually. The formation of Si-O-Ti interfacial layer plays the most important role in enhancing photocatalytic performances which is characterized by XPS and FT-IR. The narrower band gap of interfacial layer is able to tune the electronic structure, thereby inducing the charge transfer, charge separation and avoiding rapid electron-hole recombination while such enhancement will be weakened if the growth of interfacial layer gets saturation, meanwhile, the growth of SiO_2 layer starts. In addition, the red-shift in optical absorption spectra indicates a better absorption of light with a wider range of wavelengths. Combining these two factors, ALD is capable of realizing enhancement in the field of photocatalyst and suppression in the use of white pigment of photocatalytic activity. Last but not least, depositing SiO_2 on TiO_2 at room temperature is very promising not only about the easily controlled operation but the relatively high content of hydroxyl groups

compared with other operating temperatures which is vital for the decomposition of Rhodamine B under solar irradiation.

4.2 Recommendations

In this work, the growth of Si-O-Ti interfacial layer at room temperature using water vapor is hindered which is indicated in the FT-IR figure while this shortcoming may be overcame by adding catalyst such as NH_3 etc.

The enhancement of photocatalytic performance is multicriteria including the amount of hydroxyl groups, the growth of interfacial layer, the growth of SiO_2 layer, band gap of interface and quality of coating. In the field of photocatalyst, the relatively thick SiO-Ti interfacial layer while SiO_2 layer negligible is highly required which means the band gap of interfacial layer is relatively narrow and the negligible SiO_2 layer cannot block the surface for the contact between interfacial layer and air or solution. The operating temperature should be as low as possible unless it will cause condensation in ALD process like room temperature in this work to gain more hydroxyl groups which support better photocatalytic properties. In addition, annealing is a good method to promote the photocatalytic activity via modifying the roughness of interface. For the use of passivation in white pigment, the thick SiO_2 is highly recommended due to the inert nature to avoid the contact between interfacial layer or TiO_2 and environment like air or solutions.

The precise control for the growth of silica thin film is required especially for the enhancement of photocatalytic performance. Last but not least, the selection of precursors is vital because its effect on ALD processes such as operating temperature and pressure.

Appendix A

ALD Set-up

Table 0-1 Parts in ALD Set-up corresponding to Figure 2.1

Code	Part
E1 to E2	Bubbler containing precursor (E1: $SiCl_4$, E2: H_2O)
E3 to E10	Gaswashers (E4/E8 contains silicon oil, E6/E10 contains NaOH)
F1 to F2	HEPA filter for Nanoparticles in effluent
H1 to H3	Heating tape for tubing
H4 to H5	Heating mantle for bubbler E1 and E2
H6	Infrared lamp for heating reactor R1
MFC-1	Mass Flow Controller for controlling flow rate of N_2 carrier and purge gas
MFC-2	Mass Flow Controller for controlling flow rate of additional N_2 fluidization gas
R1	Reactor glass
MS	Mass Spectrometer
V3 to V4	Ball valve electronically actuated for N_2 supply through the precursor line
V5 to V6	3-way manifold valve, pneumatic, for switching between bubbling through and by-passing E1&E2
V7 to V9	Bellows sealed valve, pneumatic, for windbox feed stream (to prevent back flow into other precursor line)
V10 to V11	Bellows sealed valve, pneumatic, for exhaust stream into gas washers (to preventing mixing of $SiCl_4$ and H_2O)
CV1 to CV2	Check valve for protecting MFC-1 from back-flowing precursor
X1 to X2	Vibromotors for fluidization assistance

Appendix B

TEM Images

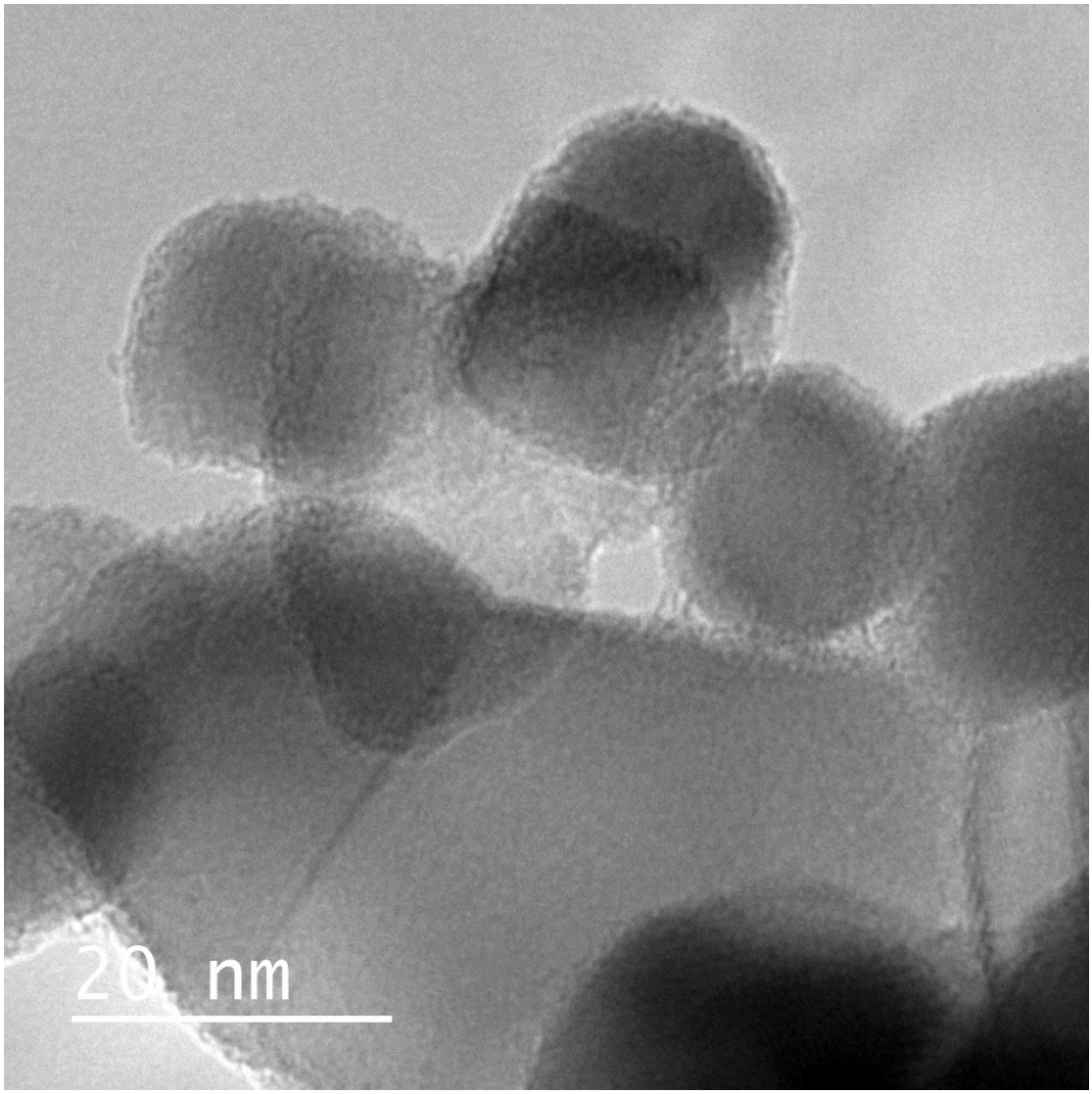

Figure 0-1 TEM Image of SiO_2 coated TiO_2 nanopowders fabricated at 100 °C for 12 cycles

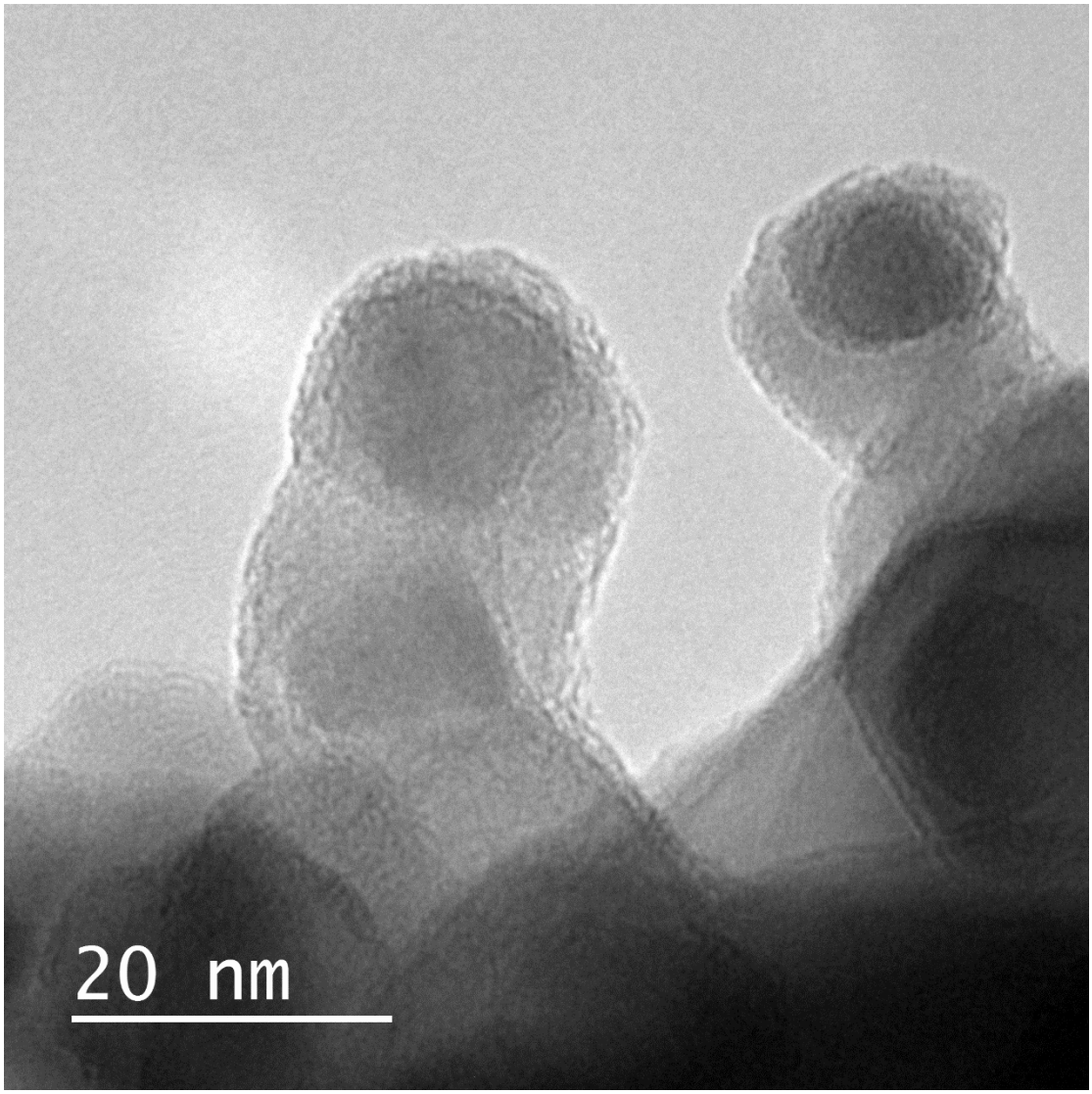

Figure 0-2 TEM Image of SiO_2 coated TiO_2 nanopowders fabricated at 100 °C for 30 cycles

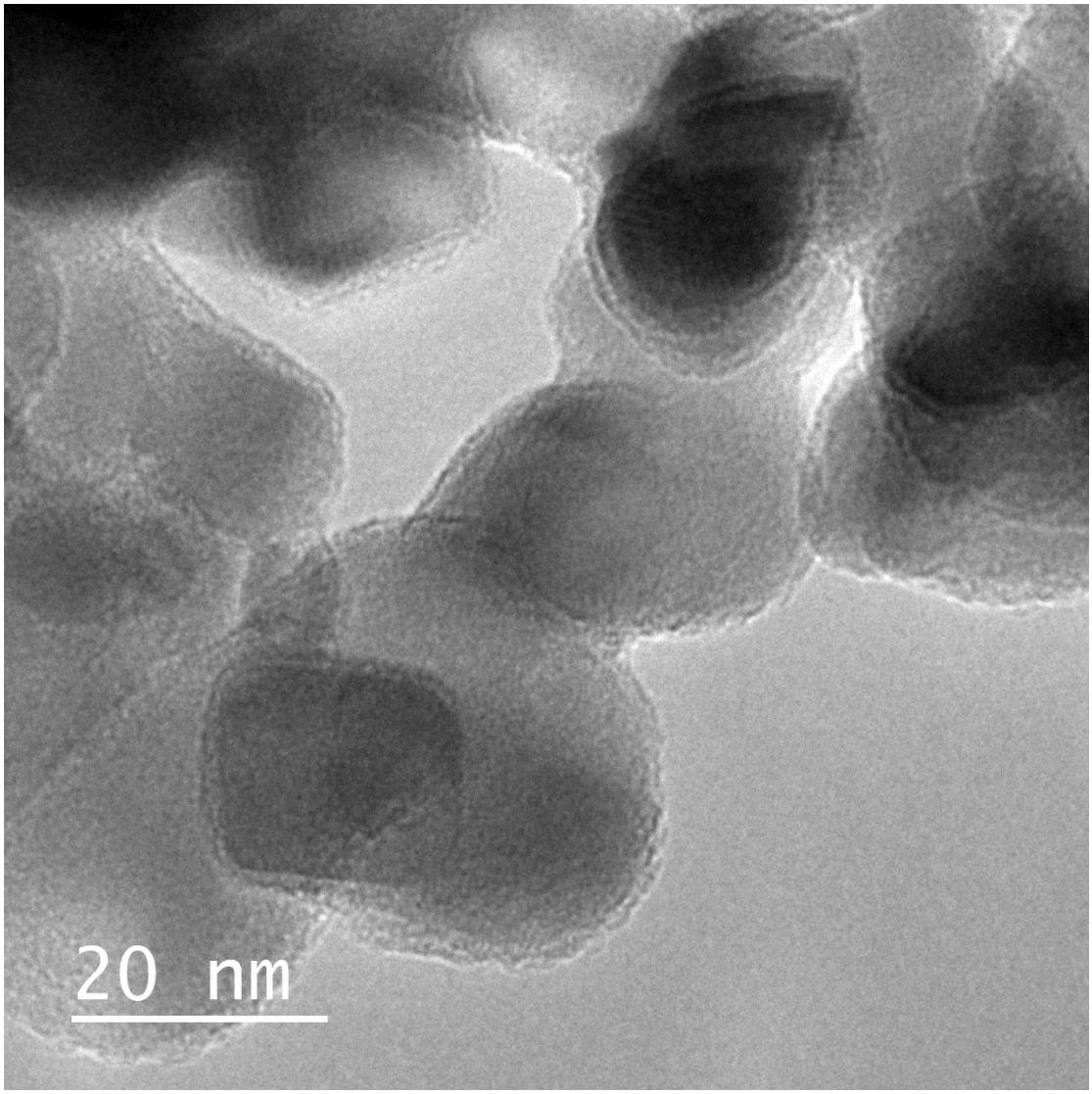

Figure 0-3 TEM Image of SiO_2 coated TiO_2 nanopowders fabricated at 100 °C for 40 cycles

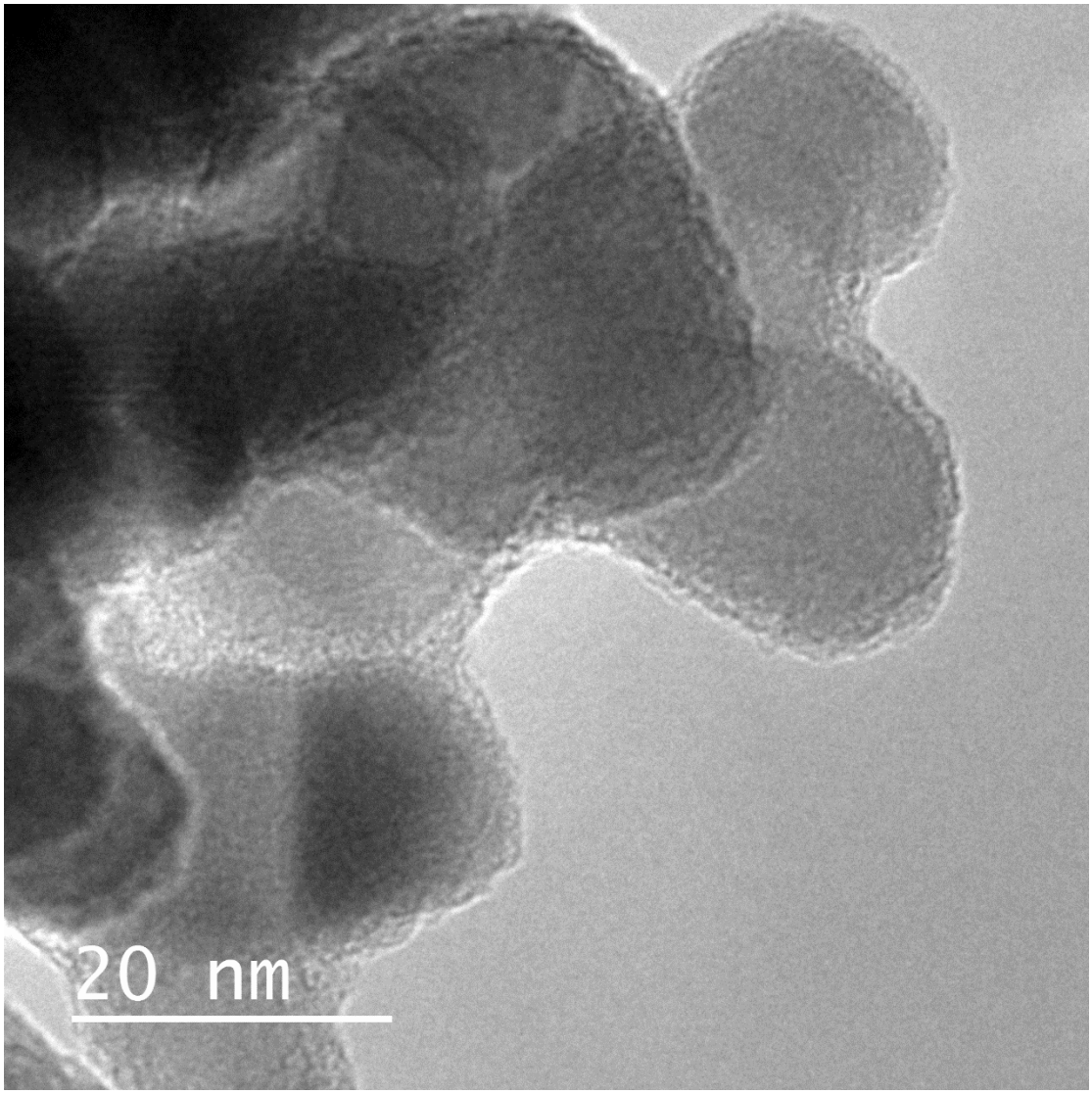

Figure 0-4 TEM Image of SiO_2 coated TiO_2 nanopowders fabricated at 200 °C for 12 cycles

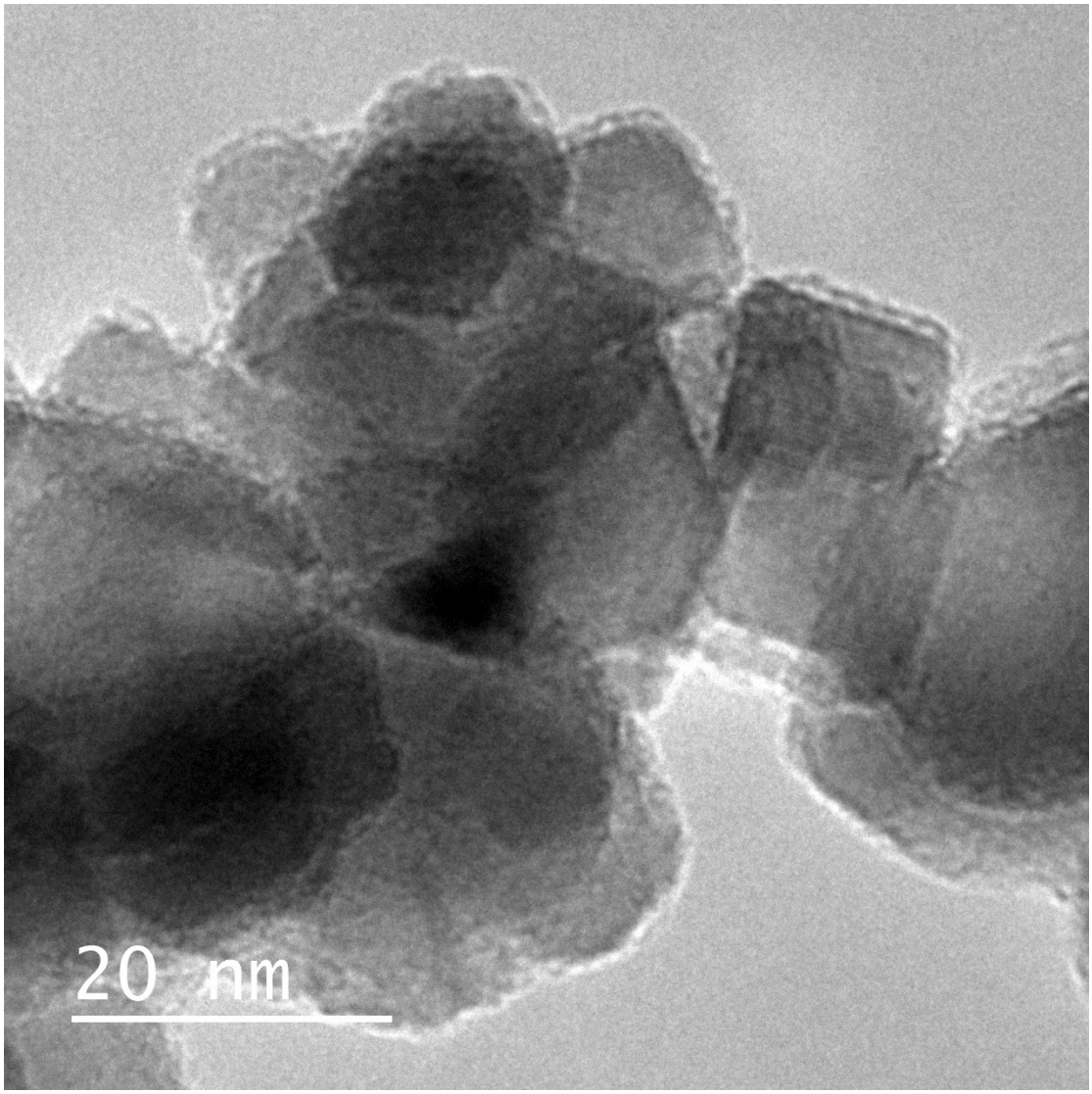

Figure 0-5 TEM Image of SiO_2 coated TiO_2 nanopowders fabricated at 250 °C for 12 cycles

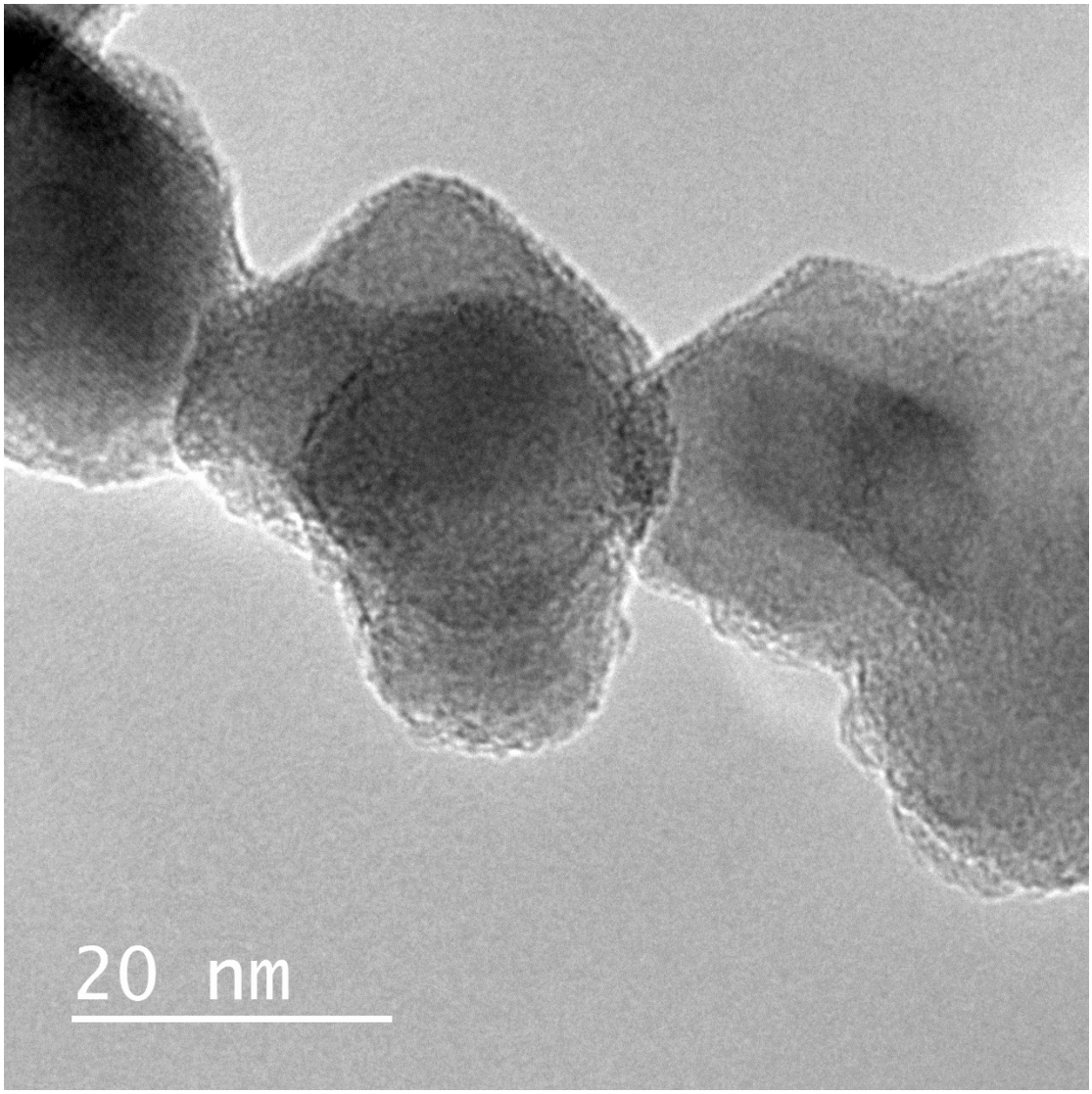

Figure 0-6 TEM Image of SiO_2 coated TiO_2 nanopowders fabricated at room temperature for 12 cycles

Appendix C

Database of INAA

Table 0-1 Si Concentration of different samples

Number	Reactor T [°C]	# cycles	Sequence [min]	Si Concentration
1	100	5	1/3/3/8	1.44
2	100	12	10s/3/3/8	1.98
3	100	8	1/3/3/8	1.8
4	200	12	20s/3/3/8	2.12
5	100	12	5s/3/3/8	2.06
6	100	20	1/3/3/8	2.5
7	200	12	5s/3/3/8	2.43
8	100	12	20s/3/3/8	1.79
9	250	12	20s/3/3/8	2.1
10	200	12	40s/3/3/8	2.43
11	100	12	40s/3/3/8	1.93
12	100	2	1/3/3/8	0.9
13	200	12	10s/3/3/8	2.13
14	100	8	1/3/3/8	1.97
15	25	12	1/3/3/8	2.9
16	100	12	1/3/3/8	2.3
17	200	12	1/3/3/8	2.6
18	250	12	1/3/3/8	2.7

Database of Photocatalytic Test

Table 0-2 Photocatalytic Test of the samples varying number of cycles at 100 °C after annealing.

Exposure Time/min	2cycles 100°C	5cycles 100°C	8cycles 100°C	12cycles 100°C	P25
-30	1	1	1	1	1
-25	0.96949	0.96628	0.95449	0.96747	0.96845
-20	0.96585	0.96303	0.95048	0.9615	0.96776
-15	0.96055	0.96057	0.94652	0.95955	0.96706
-10	0.95659	0.95838	0.94555	0.95857	0.96372
-5	0.95562	0.95762	0.94458	0.95864	0.9568
0	0.95465	0.95644	0.93616	0.95764	0.94988
5	0.24523	0.22434	0.17005	0.31265	0.642
10	0.0722	0.04952	0.02327	0.0722	0.40871
15	0.02566	0.01432	0.01193	0.02446	0.24344
20	0.00895	0.00716	0.01134	0.01909	0.11874
25					0.04117
30					0.01432

Table 0-3 Photocatalytic Test of the samples varying number of cycles at 100 °C.

Exposure time/min	RhB	P25	P25/2	2 cycles	5 cycles	8 cycles	12 cycles	30 cycles	40 cycles
-30	1	1	1	1	1	1	1	1	1
-28	1	0.81839	0.87384	0.94361	0.97875	0.91672	0.87905	0.86227	0.88252
-12	1	0.79526	0.85417	0.93361	0.97875	0.90672	0.87153	0.85359	0.85822
-5	1	0.78962	0.84838	0.92952	0.97343	0.8959	0.86516	0.84664	0.84838
0	1	0.7868	0.84606	0.91542	0.96812	0.87508	0.864	0.84606	0.84491
5	0.98843	0.58319	0.53125	0.36565	0.25634	0.2635	0.38889	0.84954	0.86169
10	0.99248	0.48393	0.35822	0.17567	0.06831	0.05791	0.14063	0.81829	0.81134
15	0.97338	0.37169	0.21238	0.07287	0.02212	0.01561	0.03241	0.76389	0.79514
20	0.98553	0.27411	0.08391	0.02863	0.00781	0.00586	0.011	0.75058	0.76447
25	0.95197	0.18105	0.03819	0.01106	0.0026	0.0026	0	0.71238	0.7228
30	0.98032	0.09814	0.01968	0.0039	0.0013	0.0013	0.00463	0.69907	0.70197
45	0.95023	--						0.53472	0.59664
105	0.875							0.0978	0.23958

Table 0-4 Photocatalytic Test of the samples varying number of cycles at room temperature.

Exposure Time/min	P25	2cycles	5cycles	8cycles	12cycles
-30	1	1	1	1	1
-25	0.97089	0.92585	0.92659	0.9242	0.90391
-20	0.96968	0.92212	0.92239	0.91737	0.89284
-15	0.96748	0.9184	0.91819	0.90055	0.89129
-10	0.96527	0.91468	0.90399	0.89137	0.88737
-5	0.95907	0.90095	0.90979	0.8909	0.88186
0	0.95286	0.88723	0.89558	0.88007	0.86635
5	0.60859	0.52804	0.46539	0.41408	0.58532
10	0.36814	0.26492	0.22136	0.20525	0.33771
15	0.19033	0.14916	0.13842	0.11396	0.22017
20	0.11635	0.09547	0.05788	0.05788	0.12709
25	0.05609	0.04057	0.03103	0.03162	0.08294
30		0.02625	0.01492	0.01909	0.05131
35		0.01498	0.00895	0.01372	0.03043

Table 0-5 Photocatalytic Test of the samples varying operating temperatures for 12 cycles.

Exposure Time/min	P25	RT	100°C	200°C	250°C	RhB
-30	1	1	1	1	1	1
-25	0.81839	0.88278	0.86405	0.85619	0.86949	1
-10	0.79526	0.8719	0.85136	0.84278	0.85752	1
-5	0.78962	0.86828	0.84713	0.83831	0.85353	1
0	0.7868	0.86465	0.8429	0.83384	0.84955	1
5	0.58319	0.58429	0.39154	0.59879	0.53172	1
10	0.48393	0.42659	0.13051	0.40242	0.28822	0.99637
15	0.37169	0.29003	0.03686	0.24109	0.13112	0.98852
20	0.27411	0.18489	0.01692	0.17341	0.05378	0.98308
25	0.18105	0.12749	0.00785	0.07674	0.02356	0.99215
30	0.09814	0.07855		0.04653	0.01208	0.99154
35		0.05378		0.03021	0.01027	0.98429
40		0.02356		0.01511		0.9861

Bibliography

1. Puurunen, Riikka L. "Surface chemistry of atomic layer deposition: A case study for the trimethylaluminum/water process." *Journal of applied physics*97.12 (2005): 9.
2. Goulas, Aristeidis, and J. Ruud van Ommen. "Atomic layer deposition of platinum clusters on titania nanoparticles at atmospheric pressure." *Journal of Materials Chemistry A* 1.15 (2013): 4647-4650.
3. Van Bui, Hao, et al. "Controlled growth of palladium nanoparticles on graphene nanoplatelets via scalable atmospheric pressure atomic layer deposition." *The Journal of Physical Chemistry C* 120.16 (2016): 8832-8840.
4. Valdesueiro, David, et al. "Gas-phase deposition of ultrathin aluminium oxide films on nanoparticles at ambient conditions." *Materials* 8.3 (2015): 1249-1263.
5. Mueller, Roger, et al. "OH surface density of SiO_2 and TiO_2 by thermogravimetric analysis." *Langmuir* 19.1 (2003): 160-165.
6. Guo, Jing, et al. "Room-temperature pulsed CVD-grown SiO_2 protective layer on TiO_2 particles for photocatalytic activity suppression." *RSC Advances* 7.8 (2017): 4547-4554.
7. Klaus, J. W., and S. M. George. "SiO_2 Chemical Vapor Deposition at Room Temperature Using $SiCl_4$ and H_2O with an NH_3 Catalyst." *Journal of the Electrochemical Society* 147.7 (2000): 2658-2664.
8. Tsapatsis, Michael, and George R. Gavalas. "A kinetic model of membrane formation by CVD of SiO_2 and Al_2O_3." *AIChE journal* 38.6 (1992): 847-856.
9. Jiang, Xirong, et al. "Application of atomic layer deposition of platinum to solid oxide fuel cells." *Chemistry of materials* 20.12 (2008): 3897-3905.
10. Pfeiffer, Kristin, et al. "Comparative study of ALD SiO_2 thin films for optical applications." *Optical Materials Express* 6.2 (2016): 660-670.
11. King, David M., et al. "Atomic layer deposition on particles using a fluidized bed reactor with in situ mass spectrometry." *Surface and Coatings Technology* 201.22 (2007): 9163-9171.
12. Kern, Werner. "The evolution of silicon wafer cleaning technology." *Journal of the Electrochemical Society* 137.6 (1990): 1887-1892.
13. Shi, Guoyue, et al. "Electrochemistry and Electrocatalytic Properties of Hemoglobin in Layer-by-Layer Films of SiO_2 with Vapor−Surface Sol−Gel Deposition." *Analytical chemistry* 79.10 (2007): 3581-3588.
14. Rha, Sa-Kyun, et al. "Characteristics of silicon oxide thin films prepared by sol electrophoretic deposition method using tetraethylorthosilicate as the precursor." *Current Applied Physics* 9.2 (2009): 551-555.
15. Vitanov, P., et al. "Low-temperature deposition of ultrathin SiO_2 films on Si substrates." *Journal*

of Physics: Conference Series. Vol. 514. No. 1. IOP Publishing, 2014.

16. Fujino, K., et al. "Doped silicon oxide deposition by atmospheric pressure and low temperature chemical vapor deposition using tetraethoxysilane and ozone." *Journal of the Electrochemical Society* 138.10 (1991): 3019-3024.
17. Boies, Adam M., et al. "SiO_2 coating of silver nanoparticles by photoinduced chemical vapor deposition." *Nanotechnology* 20.29 (2009): 295604.
18. Ma, Zhen, et al. "Surface modification of Au/TiO_2 catalysts by SiO_2 via atomic layer deposition." *The Journal of Physical Chemistry C* 112.25 (2008): 9448-9457.
19. Kim, Jae-Kyung, et al. "Atomic Layer Deposition of SiO_2 Thin Films Using Tetrakis (ethylamino) silane and Ozone." *Journal of nanoscience and nanotechnology* 12.4 (2012): 3589-3592.
20. King, David M., et al. "Passivation of pigment-grade TiO_2 particles by nanothick atomic layer deposited SiO_2 films." *Nanotechnology* 19.25 (2008): 255604.
21. Kumar, Manippady Krishna, et al. "Field effects in plasmonic photocatalyst by precise SiO_2 thickness control using atomic layer deposition." *Acs Catalysis* 1.4 (2011): 300-308.
22. Dingemans, Gijs, et al. "Plasma-assisted atomic layer deposition of low temperature SiO_2." *ECS Transactions* 35.4 (2011): 191-204.
23. Kang, Jeung Ku, and Charles B. Musgrave. "Mechanism of atomic layer deposition of SiO_2 on the silicon (100)-2×1 surface using $SiCl_4$ and H_2O as precursors." *Journal of applied physics* 91.5 (2002): 3408-3414.
24. Burton, B. B., et al. "SiO_2 atomic layer deposition using tris (dimethylamino) silane and hydrogen peroxide studied by in situ transmission FTIR spectroscopy." *The Journal of Physical Chemistry C* 113.19 (2009): 8249-8257.
25. Lawless, D., N. Serpone, and D. Meisel. "Role of hydroxyl radicals and trapped holes in photocatalysis. A pulse radiolysis study." *The Journal of Physical Chemistry* 95.13 (1991): 5166-5170.
26. Lee, H. S., S. M. Koo, and J. W. Yoo. "TiO_2–SiO_2 Nanoparticles for Suppressing Photocatalytic Activities and Improving Hydrophilicity." *J. Ceram. Process. Res* 13 (2012): S300-S303.
27. Ding, Z., G. Q. Lu, and P. F. Greenfield. "Role of the crystallite phase of TiO_2 in heterogeneous photocatalysis for phenol oxidation in water." *The Journal of Physical Chemistry B* 104.19 (2000): 4815-4820.
28. Wu, Zhizhong, et al. "Structural color in porous, superhydrophilic, and self-cleaning SiO_2/TiO_2 Bragg stacks." *Small* 3.8 (2007): 1445-1451.
29. Lassaletta, G., et al. "Spectroscopic characterization of quantum-sized TiO_2 supported on silica-influence of size and TiO_2- SiO_2 interface composition." *Journal of Physical Chemistry* 99.5 (1995): 1484-1490.
30. Fu, Xianzhi, et al. "Enhanced photocatalytic performance of titania-based binary metal oxides: TiO_2/ SiO_2 and TiO_2/ZrO_2." *Environmental Science & Technology* 30.2 (1996): 647-653.
31. Doolin, P. K., et al. "Acidity studies of titania-silica mixed oxides." *Catalysis letters* 25.3-4 (1994): 209-223.

32. Anderson, Carl, and Allen J. Bard. "Improved photocatalytic activity and characterization of mixed TiO_2/SiO_2 and TiO_2/Al_2O_3 materials." *The Journal of Physical Chemistry B* 101.14 (1997): 2611-2616.
33. Valdesueiro, David, et al. "Gas-phase deposition of ultrathin aluminium oxide films on nanoparticles at ambient conditions." *Materials* 8.3 (2015): 1249-1263.
34. van Ommen, J. Ruud, Jose Manuel Valverde, and Robert Pfeffer. "Fluidization of nanopowders: a review." *Journal of Nanoparticle Research* 14.3 (2012): 737.
35. Erdem, Bedri, et al. "XPS and FTIR surface characterization of TiO_2 particles used in polymer encapsulation." *Langmuir* 17.9 (2001): 2664-2669.
36. Chen, Feng, Jincai Zhao, and Hisao Hidaka. "Highly selective deethylation of rhodamine B: Adsorption and photooxidation pathways of the dye on the TiO_2/SiO_2 composite photocatalyst." *International Journal of Photoenergy* 5.4 (2003): 209-217.
37. Fujishima, Akira. "Electrochemical photolysis of water at a semiconductor electrode." *nature* 238 (1972): 37-38.
38. Hashimoto, Kazuhito, Hiroshi Irie, and Akira Fujishima. "TiO_2 photocatalysis: a historical overview and future prospects." *Japanese journal of applied physics* 44.12R (2005): 8269.
39. Kumar, S. Girish, and L. Gomathi Devi. "Review on modified TiO_2 photocatalysis under UV/visible light: selected results and related mechanisms on interfacial charge carrier transfer dynamics." *The Journal of Physical Chemistry A* 115.46 (2011): 13211-13241.
40. Schneider, Jenny, et al. "Understanding TiO_2 photocatalysis: mechanisms and materials." *Chemical reviews* 114.19 (2014): 9919-9986.
41. Park, Hyunwoong, et al. "Surface modification of TiO_2 photocatalyst for environmental applications." *Journal of Photochemistry and Photobiology C: Photochemistry Reviews* 15 (2013): 1-20.
42. Xie, Shunji, et al. "Photocatalytic reduction of CO_2 with H_2O: significant enhancement of the activity of $Pt–TiO_2$ in CH_4 formation by addition of MgO." *Chemical communications* 49.24 (2013): 2451-2453.
43. Sneh, O., et al. "Atomic layer growth of SiO_2 on Si (100) using $SiCl_4$ and H_2O in a binary reaction sequence." *Surface Science* 334.1-3 (1995): 135-152.
44. Guo, Jing, et al. "Room-temperature pulsed CVD-grown SiO_2 protective layer on TiO_2 particles for photocatalytic activity suppression." *RSC Advances* 7.8 (2017): 4547-4554.
45. Chao, S. S., et al. "Chemical states study of Si in SiO_x films grown by PECVD." *Applied Surface Science* 26.4 (1986): 575-583.
46. Park, Ok Kyung, and Young Soo Kang. "Preparation and characterization of silica-coated TiO_2 nanoparticle." *Colloids and Surfaces A: Physicochemical and Engineering Aspects* 257 (2005): 261-265.
47. Yuan, Lan, et al. "Origin of enhancing the photocatalytic performance of TiO_2 for artificial photoreduction of CO_2 through a SiO_2 coating strategy." *The Journal of Physical Chemistry C* 120.1 (2015): 265-273.

48. Biesinger, Mark C., et al. "Resolving surface chemical states in XPS analysis of first row transition metals, oxides and hydroxides: Cr, Mn, Fe, Co and Ni." *Applied Surface Science* 257.7 (2011): 2717-2730.
49. Wang, Shurong, Fei Teng, and Yunxuan Zhao. "Effect of the molecular structure and surface charge of a bismuth catalyst on the adsorption and photocatalytic degradation of dye mixtures." *RSC Advances* 5.93 (2015): 76588-76598.
50. Anderson, Carl, and Allen J. Bard. "An improved photocatalyst of TiO_2/SiO_2 prepared by a sol-gel synthesis." *The Journal of Physical Chemistry* 99.24 (1995): 9882-9885.
51. Gallas, Bruno, et al. "SiO_2–TiO_2 interfaces studied by ellipsometry and x-ray photoemission spectroscopy." *Journal of applied physics* 92.4 (2002): 1922-1928.
52. Yang, Kesong, Ying Dai, and Baibiao Huang. "First-principles calculations for geometrical structures and electronic properties of Si-doped TiO_2." *Chemical Physics Letters* 456.1 (2008): 71-75.
53. Sasahara, Akira, Chi Lun Pang, and Masahiko Tomitori. "Atomic Scale Analysis of Ultrathin SiO_2 Films Prepared on TiO_2 (100) Surfaces." *The Journal of Physical Chemistry C* 114.47 (2010): 20189-20194.
54. Chao, S. S., et al. "Chemical states study of Si in SiO_x films grown by PECVD." *Applied Surface Science* 26.4 (1986): 575-583.
55. Li, Gang, Fang Liu, and Zhao Zhang. "Enhanced photocatalytic activity of silica-embedded TiO_2 hollow microspheres prepared by one-pot approach." *Journal of Alloys and Compounds* 493.1 (2010): L1-L7.
56. Xu, Yue-hua, and Zhuo-xian Zeng. "The preparation, characterization, and photocatalytic activities of Ce-TiO_2/SiO_2." *Journal of Molecular Catalysis A: Chemical 279.1* (2008): 77-81.
57. Lin, C-P., et al. "Effect of annealing temperature on the photocatalytic activity of TiO_2 thin films." *Energy Procedia* 34 (2013): 627-636.
58. Ferguson, J. D., et al. "ALD of SiO_2 at Room Temperature Using TEOS and H_2O with NH_3 as the Catalyst." *Journal of The Electrochemical Society* 151.8 (2004): G528-G535.
59. Gu, Wei, and Carl P. Tripp. "Role of water in the atomic layer deposition of TiO_2 on SiO_2." *Langmuir* 21.1 (2005): 211-216.

Glossary

List of Acronyms

ALD Atomic Layer Deposition

FBR Fluidizaed Bed Reactor

TEM transmission electron microscopy

FTIR Fourier Transform Infrated Spectroscopy

GPC Growth Per Cycle

TGA Thermogravimetric Analysis

UV-vis UltravioletâASvisible spectroscopy

BET Brunauer–Emmett–Teller Method

TEOS Tetraethylorthosilicate

INAA Instrumental Neutron Activation Analysis